Constitutive modeling the elasto-viscoplastic behavior of Regina clay soil under the drained stress path condition

Yiwei Luo

A Thesis

In

The Department

Of

Building, Civil, and Environmental Engineering

Presented in Partial Fulfillment of the Requirements

For the Degree of

Master of Applied Science (Geotechnical Engineering) at

Concordia University

Montréal, Québec, Canada

March 2019

© Yiwei Luo, 2019

CONCORDIA UNIVERSITY

School of Graduate Studies

This is to certify that the thesis prepared

By: **Yiwei Luo**

Entitled: **Constitutive modelling the elasto-viscoplastic behavior of Regina clay soil under the drained stress path condition**

and submitted in partial fulfillment of the requirements for the degree of

Master of Applied Science (Geotechnical Engineering)

complies with the regulations of the University and meets the accepted standards with respect to originality and quality.

Signed by the final Examining Committee:

Chair and Examiner

Dr. Adel M. Hanna

Examiner

Dr. Ayhan Ince

Examiner

Dr. Attila Michael Zsaki

Supervisor

Dr. Biao Li

Approved by: _____Chair of the Department or Graduate Program Director

_____Dean of Faculty

Date:

ABSTRACT

The stress–strain behavior of soft clay soil is dependent on the applied strain rate and such time dependency behavior should be considered in geotechnical engineering projects such as the bearing capacity analysis for a foundation. Most previous studies focus on elastic-viscoplastic behavior of clay soil under an undrained stress path condition. The developed constitutive models cannot simulate the strong time-dependent stress-strain relation of soft clay under the drained stress path condition. In the long-term bearing capacity analysis for a shallow foundation, the neglect of the time-dependent stress-strain relation of soft clay may result in inaccurate result.

In this study, the strain-rate-dependent soil behavior is modeled using the Drucker-Prager/Cap model with the consideration of soil creep behavior. Both consolidation creep and shear creep mechanisms are considered in the modeling. A simplified approach is proposed to derive creep parameters from stress relaxation test results. The constitutive modeling is validated against experimental measurements on strain-rate-dependent behavior of Regina clay soil under the drained stress path condition. Finite element modeling on the long-term bearing capacity of a shallow foundation on soft clay is also performed. The result shows that the considering of viscoplastic behavior of clay soils does not affect the ultimate bearing capacity. However, it yields the lower bound of developed shear stress of a shallow foundation at a given vertical displacement, which is to be conservative from the engineering point of view.

Keywords: Drucker-Prager/Cap model, time-dependent stress-strain relation, finite element modeling, bearing capacity analysis

ACKNOWLEDGEMENT

First, I would like to express my heartfelt thanks to Professor Biao Li, my thesis supervisor, for his tireless effort in teaching, assisting, guiding and advising me throughout this research.

I am grateful to the support provided by my family members and friends at difficult times during this whole period.

I would like to thank the support by NSERC Discovery Grant Canada (NO. RGPIN-2017-05169).

I would also thank the examination committee for reading this thesis and providing critical comments.

Finally, I would like to acknowledge the financial support received from the Department of Building, Civil, and Environmental Engineering at University of Concordia to make this research possible.

Contents

ABSTRACT ii

ACKNOWLEDGEMENT iii

List of Figures vii

List of Tables x

List of Symbols xi

1. Introduction 1

1.1. Background 1

1.2. Objectives of the Current Study 2

1.3. Structure of thesis 3

1.4. Original Contributions 3

2. Literature Review 4

2.1. Experimental study 4

2.1.1. Background 4

2.1.2. Limitations on investigations 6

2.2. Elastoplastic soil models 7

2.2.1. Introduction 7

2.2.2. Modified Cam clay model 8

2.2.3. Modified Drucker-Prager/Cap Model 8

2.2.4. Lade's Single Hardening Model 8

2.3. Elastic Viscoplastic Models 9

2.3.1. Hypothesizes 9

2.3.2. Semilogarithmic Creep Law 10

2.3.3. Perzyna Viscoplastic Model 11

2.3.4. Bjerrum's assumption 12

2.3.5. Singh-Mitchell Model 13

2.3.6. Tavenas Model 14

2.3.7. Leroueil Framework 15

2.3.8. Yin and Gracham model 17

3. Drucker-Prager/Cap model and Singh-Mitchell model 19

3.1. General introduction 19

3.2. Stress and strain 19

3.3. Elastoplastic theory 21

3.4. Modified Drucker-Prager/Cap model 24

For shear yielding 31

For cap hardening 31

3.5. Singh-Mitchell model 32

4. Deriving creep parameters based on stress relaxation tests 39

4.1. Introduction 39

4.2. Consolidation creep parameters 39
4.3. Shear creep parameters 41
4.4. Deriving creep parameters for Regina clay soil 43
5. Numerical modeling of tri-axial tests on Regina clay soil 47
5.1. Tri-axial tests on Regina clay soil 47
5.2. FEM modeling 50
5.3. Summary 59
6. Bearing capacity analysis of a strip foundation 60
6.1. Analytical solution based on Terzaghi's bearing capacity equation 60
6.2. FEM modeling 63
6.3. Comparison and summary 75
7. Conclusions and recommendations for future work 77
7.1. Conclusion 77
Deriving creep parameters from relaxation tests 77
Constitutive modeling on elasto-viscoplastic behavior of Regina clay 77
Bearing capacity analysis of a strip foundation 78
7.2. Recommendations for Future Work 78
References 79

List of Figures

Figure 2-1 Typical CRS oedometer tests on Batisean day, from Leroueil et al. (1985). 11

Figure 2-2 Geological history and compressibility of a young and an aged normally consolidated clay, from Liingaard et al. (2004). 13

Figure 2-3 Creep curves predicted by the stress–strain–time functions, from Liingaard et al. (2004). 14

Figure 2-4 Special CRS oedometer tests on Batiscan clay, from Leroueil et al. (1985). 15

Figure 3-1 Stress-strain path for a real soil, from Bjerre (2015). 22

Figure 3-2 Yield surfaces of the modified cap model in the meridional (p–q) plane, after Abaqus (2016). 25

Figure 3-3 Projection of the modified cap yield/flow surfaces, after Abaqus (2016). 27

Figure 3-4 Flow potential of the modified cap model in the p–t plane, after Abaqus (2016). 28

Figure 3-5 Typical cap hardening behavior, from Abaqus (2016). 29

Figure 3-6 Regions of activity of shear and consolidation creep mechanisms, after Abaqus (2016). 33

Figure 3-7 Equivalent creep stress for shear creep, after Abaqus (2016). 34

Figure 3-8 Creep potentials: shear mechanism, after Abaqus (2016). 35

Figure 3-9 Creep potentials: consolidation mechanism, after Abaqus (2016). 35

Figure 4-1 Sketch showing the stress path of a relaxation test. 42

Figure 4-2 Result of stress relaxation test conducted during the oedometer test on Regina clay sample, after Hewage (2018). 43

Figure 4-3 Result of stress relaxation test conducted during the shear stage of drained triaxial compression test on Regina clay sample, after Hewage (2018). 44

Figure 4-4 Stress path of two relaxation tests under the drained triaxial testing condition. 44
Figure 5-1 (a) Automatic volume change devices; (b) GDS pump, from Hewage (2018). 48
Figure 5-2 Schematic diagram of triaxial system used for drained triaxial compression tests on saturated soils, from Hewage (2018). 49
Figure 5-3 Measured strain-rate-dependent stress-strain relation of Regina clay soil, after Hewage (2018). 49
Figure 5-4 Sketch showing the configuration, mesh, and one monitoring points of the studied problem. 51
Figure 5-5 Boundary conditions of the finite element. 51
Figure 5-6 Modeled Mises stress (in Pa) distributions in Regina clay soil using (a) 0.966 day and (b) 24.138 days. 52
Figure 5-7 Modeled plastic strain distributions in Regina clay soil using (a) 0.966 day and (b) 24.138 days. 53
Figure 5-8 Modeled creep strains in Regina clay soil using (a) 0.966 day and (b) 24.138 days. . 54
Figure 5-9 Modeled stress paths of monitoring point 1 in p–q space. 54
Figure 5-10 Modeled and measured stress-strain relations for a Regina clay sample. 55
Figure 5-11 Modeled volumetric-axial strain relations for numerical tests under different strain rates. 56
Figure 5-12 Modelled total-creep axial strain relations for numerical tests under different strain rates. 56
Figure 5-13 Relationship between equivalent stress and axial strain by different strain rates. 58
Figure 6-1 Sketch showing a typical shallow foundation, from Helwany (2007). 61

Figure 6-2 General shear failure of a strip foundation: Terzaghi's assumptions, from Terzaghi (1951). 61
Figure 6-3 Sketch showing the configuration, mesh, and two monitoring points of the studied problem. 64
Figure 6-4 Relationship between the height and mean effective stress. 65
Figure 6-5 Modeled plastic shear strain distributions in Regina clay soil using (a) one day (b) 30 days (c) 60 days. 68
Figure 6-6 Modeled load-displacement curve for the studied footing problem using different time intervals. 69
Figure 6-7 Modeled Mises stress (in Pa) distributions in Regina clay soil using (a) one day (b) 30 days (c) 60 days. 71
Figure 6-8 Modeled total volumetric inelastic strain in Regina clay soil using (a) one day (b) 60days (PEQC4 stands for volumetric inelastic strain in Abaqus). 72
Figure 6-9 Modeled creep strain in Regina clay soil using (a) one day (b) 60days (CE2 stands for creep strain in vertical direction in Abaqus). 72
Figure 6-10 Modeled reaction force in Regina clay soil using (a) one day (b) 60days (RF2 stands for reaction force in vertical direction in Abaqus). 73
Figure 6-11 Modeled equivalent plastic strains for Drucker-Prager failure surface in Regina clay soil using (a) one day (b) 60days (PEQC1 stands for equivalent plastic strains for Drucker-Prager failure surface in Abaqus). 74
Figure 6-12 Modeled stress paths of (a) monitoring point 1 (b) monitoring point 2 (c) monitoring point 3 in p–q space (d) monitoring point 4 in p–q space in p–q space. 75
Figure 6-13 FEM results and the Terzaghi's results for the bearing capacity. 76

List of Tables

Table 3-1 Failure and plastic potential functions for the time-independent plastic behavior..... 26

Table 3-2 Equivalent creep stresses and plastic potential functions for creep behavior. 34

Table 4-1 Material properties for constitutive modelling on Regina clay. 45

Table 5-1 Step information of relaxation tests in Abaqus. 57

List of Symbols

B	The foundation width
CRS	Constant rate of strain
D	Elastic stiffness matrix
$[D]_{ep}$	The elastoplastic stiffness matrix
E	Young's modulus
EVP	Elastic viscoplastic
F	Yielding surface
G	The elliptical portion
I	Identity matrix
I	The unit vector
K	The parameter to control the shape of yielding surface
OCR	Overconsolidation ratio
Q	The plastic potential
R	A material parameter that controls the shape of the cap
c	The cohesion strength
c'	The cohesion intercept of soil
$d\lambda$	The plastic multiplier
$d\varepsilon_s^{cr}$	A cohesion mechanism

$d\varepsilon_c^{cr}$	A consolidation mechanism
eEOP	Void ratio at the end of primary consolidation
k	Rebound indice
κ	The slope of the critical-state line
p	The mean stress
Pa	An evolution parameter which controls the hardening–softening behavior
P_b	The mean effective (yield) stress
q	The overburden pressure at foundation depth
q_u	The bearing capacity for a square foundation
r	The third invariant of deviatoric stress
γ	The unit weight of soil
t_1	The initial time
μ	Lame´s constant
ν	Poisson's ratio
λ	The slope of the normal consolidation line
λ	Lame´s constant
λ_c	Compression indice
β	Angle of friction
φ	Soil friction angle
ϕ'	The soil friction angle
σ	Stress

$\sigma_1^{'}$	Effective stress in axial direction
$\sigma_3^{'}$	Effective stress in lateral direction
σ_{cr}	The equivalent creep stress
ε	Strain
ε^e	The elastic strain
ε^p	The time-independent plastic strain
ε^{cr}	The creep strain
ε_v	The volumetric strain
ε_q	The deviatoric strain
Δt	The time interval
$\Delta\varepsilon_{11}$	Total axial strain
$\Delta\varepsilon_{11}^{cr}$	Creep strains along the axial direction of sample
$\Delta\varepsilon_{22}^{cr}$	Creep strains along the radical direction of sample
$\Delta\varepsilon_{11}^{ep}$	The axial strain due to elastoplastic deformation
$\Delta\varepsilon_{22}^{ep}$	The radial strain increment
$\Delta\varepsilon_{22}^{e}$	Radial strain due to elastic deformation
$\Delta\varepsilon_{22}^{p}$	Radial strain due to time-independent plastic deformation

$\Delta\sigma_{11}$	The axial stress increment

1. Introduction

1.1. Background

Due to the rapid growth of infrastructure and transportation development, the construction on soft soil deposits has become increasingly important in the past decade (Karim and Gnanendran 2008， Yin et al. 2011， Fang 2013). The behavior of sensitive soft clay is remarkably complicated because of the low shear strength, strain-rate dependent, high water content and large time-dependent deformations (Picornell and Nazarian 1992， Suhonen 2018). For example, light infrastructure buried in the Regina clay are often subjected to severe distress during their service life (Vu et al. 2007).

The mechanical behavior of soft clay soil is highly dependent on the applied stress path and strain rate, which makes soft clay soils display strong viscoplastic behavior (Fodil et al. 1998， Yin and Graham 1999， Yin et al. 2011). In order to properly analyze some geotechnical problems related to the viscoplastic behavior of soft clay soils, a large number of researchers focused on the creep, the stress relaxation, and the strain-rate dependent behaviors in clay soils (Fredlund 1967， Picornell and Nazarian 1996， Liingaard et al. 2004， Marques et al. 2004). Perzyna (1963) proposed some preliminary models which were based on elastic viscoplastic framework to study this behavior. Bjerrum (1967) provided a time line model to better describe this situation. Tavenas (1977) proposed a qualitative model (YLIGHT) of the clay behavior to observe the relationship between stress, strain and time. However, most previous studies focus on elastic-viscoplastic behavior of clay soil under an undrained stress path condition (Yin and Graham 1999， Yin et al. 2010， Yin et al. 2011).

The developed constitutive models cannot simulate the strong time-dependent stress-strain relation of soft clay under the drained stress path condition. An accurate characterization of the complex shear and consolidation behavior of clay soil is critical for a solve geotechnical problems (Taiebat and Carter 2000). For example, in the long-term bearing capacity analysis for a shallow foundation or the long-term stability analysis of a clay slope, the neglect of the time dependent stress-strain relation of soft clay may result in inaccurate result.

1.2. Objectives of the Current Study

During the last decades, the big amount of model has been carried out to investigate various aspects of time effect on the strength-deformation behavior of soils under undrained condition. The aim of the thesis is to develop a numerical tool for modelling the viscoplastic behavior of soft sensitive clays under the drained stress path condition and performed finite element modeling on the bearing capacity of a shallow foundation on soft clay using Drucker-Prager/Cap model combined with Singh-Mitchell creep model, to derive a more accurate bearing capacity. The specific objectives of the research are shown in the following:

1) Introducing constitutive models on describing viscoplastic behavior of soft clay with the consideration of consolidation yielding and shear yielding behaviors.
2) Deriving creep parameters from experimental work.
3) Putting into the implementation of the constitutive model using numerical tools.
4) Performing numerical analysis of a traditional footing problem considering drained viscoplastic behavior.

1.3. Structure of thesis

This thesis has been prepared according to the guidelines of the Faculty of Graduate Studies at Concordia University. It comprises seven chapters. The purpose of this work is to perform constitutive modeling on the elasto-viscoplastic behavior of Regina clay soil under the drained stress path condition. Chapter 1 includes the background and brief content about thesis. Chapter 2 contains the basics of the modelling the behavior of soft clay by composing literature reviews about different stress-strain theories and models. Chapter 3 introduces the constitutive model which contains the Drucker-Prager/Cap plastic model combined with Singh-Mitchell creep model. Chapter 4 tells about the approach of parameter identification from experimental results. Chapter 5 focus on modeling drained tri-axial tests on small samples by using ABAQUS. In chapter 6, numerical modelling bearing capacity of a strip foundation is presented. The numerical modeling results can be found in Chapter 5, 6 and conclusions and recommendations for further work are presented in Chapter 7.

1.4. Original Contributions

Previous researches did not pay enough attentions on the strain-rate dependent consolidation or shear behavior of clay soils under the drained stress path condition. The neglecting of strain-rate dependent shear behavior of clay soil under the drained stress path condition could result in an underestimate of the risks related to geotechnical engineering problems. In this research, constitutive modelling viscoplastic behavior of clay soils under the drained stress path condition will be investigated. In addition, in order to minimize the experimental procedures and time, an innovative approach is proposed to derive creep parameters from stress relaxation test results.

2. Literature Review

The published studies on analyzing the viscoplastic behavior of clay soils by conducting experimental work and theoretical modeling are presented separately in this chapter.

2.1. Experimental study

2.1.1. Background

Viscoplasticity is a behavior which describes (strain) rate-dependent non-recoverable behavior. The relaxation tests, creep tests and stress-strain tests can satisfactorily characterize the viscoplastic behavior (Yin et al. 2006).

Creep is defined as the increase in the deformation with time under a constant effective stress. The stress-strain behavior of many soft clays is strongly time-dependent, which can affect the stress distribution, deformation, and capacity of foundation soils beneath embankments, oil tanks, silos, etc., especially when the stresses are high enough to cause yielding (Yin and Graham 1989，Kurz 2014). Therefore, creep is a result of time and plastic deformation.

Lacerda (1973) and his team conducted a series of stress relaxation tests during a constant rate of strain consolidated undrained triaxial compression tests on several different clayey soils. They observe the relationship between initial time delay and strain rate prior to stress relaxation tests.

Tavenas et al. (1978) in Laval University investigated on a marine silty clay in Quebec City using triaxial tests. During their tests, special treatments were conducted to reduce the leakage due to osmosis through the membrane. All tests were carried out on small samples which were firstly reconsolidated to the in situ stress condition, and with a back pressure equivalent to the in

situ hydrostatic pore pressure. Both drained and undrained tests were carried out over durations of 100 000 min, but the results were considered to be acceptable only for the first 4000 min for the undrained tests because of the leakage. Vertical deformations and volume changes or pore pressures were measured at regular intervals in the triaxial tests. The primary consolidation is greatly diminished and the observed behavior is essentially representative of secondary consolidation or creep in their experimental work. They also conducted a series of long duration odometer consolidation tests.

In order to analysis the effects on the strain rate and viscoplastic strain on consolidation of natural clay, Kabbaj et al. (1988) performed an experimental test under an embankment built on soft clay in Quebec, which combined process of pore pressure during the consolidation. The test embankment has a diameter of 24 m at the crest and a height of 2.4 m, it was built in 4 days, with 30 cm of fill applied in the morning and the same height in the afternoon for this oedometer test.

Marques et al. (2004) performed a special laboratory test program on the St-Roch-de-l'Achigan clay, to study the behavior of creep on the different temperatures and strain rates. Their practical work included special incremental loading oedometer tests, constant rate of strain (CRS) oedometer tests performed at different strain rates, isotropic and anisotropic triaxial compression tests, and undrained shear tests. All these tests were performed under a constant temperature, varying from 10 to 50 °C. From test results, they found the vertical yield stresses and the entire limit state curve are dependent on strain rate and temperature.

Hicher (2016) conducted his experimental study on the clay from an earth dam core under complex loading condition to study a very pronounced time-dependent behavior because of the soil viscous properties. There are two rounds of tests have been performed on a compacted clay. The first round consists of constant-strain-rate compression, stress relaxation and creep. The

second round of test was performed at different levels of stress and strain in triaxial loading–unloading–reloading phases which consisting of creep and stress-relaxation tests.

Several experimental tests which includes odometer compression tests, drained triaxial compression tests and undrained triaxial tests were also conducted by Hewage (2018) to investigate numerous factors affecting the time-dependent compression behavior of Calgary clay and Regina clay, especially for relaxation and creep phenomenon.

2.1.2. Limitations on investigations

Numerous investigations have been proposed on the effects of time on the strength and deformation behavior of soft clays. However, there are limitations in the investigations.

Firstly, geologists have followed the classical pattern of separating the problems of stability, which investigated by means of strength tests. Then two types of long-term-time effects have been separately defined and investigated: creep as related to strength problems and secondary consolidation as related to settlements, however, there is practically no interconnection has been established even in the similarity of the phenomena.

Secondly, the problem of creep has been dealt with essentially as a theoretical exercise aimed at the proposal of various rheological models and it has been poorly related to in situ problems. For example, the majority of investigations, at least in North America, have been conceived with undrained creep tests. However, in all field situations partial or full drainage can develop (Tavenas et al. 1978).

Thirdly, with few exceptions, most studies focus on whether the effect of strain rates or the effect of temperature. However, the influence of anisotropy of natural clays and of microstructure was not considered in the experimental work (Marques et al. 2004).

2.2. Elastoplastic soil models

2.2.1. Introduction

In order to analysis the stress-strain behavior of soft clay, it is necessary to propose some theoretical soil models to simulate the stress-strain-time relation. Since 1960's, an increasing effort has been devoted to develop a more comprehensive description of soil behavior. Numerous formulations which are based on experimental findings and embodied in numerical methods have been proposed in the soil mechanics literature and considerable attentions have been given to the development of constitutive equations for soil. For example, the finite element method is a significant aspect of soil mechanics. Constitutive models allow engineers to solve various types of geotechnical engineering problems, especially problems that are inherently complex and cannot be solved using traditional analysis without making simplifying assumptions (Helwany 2007).

Soils are full of discrete particles, and most soil models assume that continuous stresses and strains can represent the forces and displacements within these particles. These stress–strain constitutive laws are normally fitted to experimental measurements which performed on specimens.

Elastic strains will produce when an elastic material is subjected to load. Elastic strains are reversible when the load is removed. However, if a plastic material is subjected to a load, it will sustain both elastic and plastic strains. Even the load is removed, the material will still sustain permanent plastic (irreversible) strains, no matter the elastic strains are recovered or not.

An elastic-plasticity model includes three sections: (1) a yield criterion which predicts whether the material should respond elastically or plastically because of a loading increment, (2) a strain hardening rule which controls the shape of the stress–strain response during plastic

straining, and (3) a plastic flow rule which determines the direction of the plastic strain increment that caused by a stress increment.

2.2.2. Modified Cam clay model

Modified Cam clay model is capable of describing the stress–strain behavior of soils, especially, the models can predict the pressure-dependent soil strength and the compression and dilatancy (volume change) which caused by shearing. The model can predict unlimited soil deformations without changes in stress or volume when the critical state is reached, because the models are based on critical-state theory (Roscoe and Burland 1968).

The modified Cam clay model formulations are based on the triaxial stress condition in which the intermediate and the principal minor stresses are equal ($\sigma 2 = \sigma 3$). This model is particularly useful for problems which involves three-dimensional stress conditions and plane strain conditions that are common in geotechnical engineering.

2.2.3. Modified Drucker-Prager/Cap Model

A considerable amount of finite element analysis has been conducted for a variety of geotechnical engineering applications by using the Drucker–Prager/cap plasticity model. The cap model is capable of including the effect of stress history, stress path, dilatancy, and the effect of the intermediate principal stress (Helwany 2007).They are multi-surface plasticity models, which used most frequently with an associated flow rule. The cap may harden or soften that is coupled to the Drucker-Prager yield surface (Resende and Martin 1985).

2.2.4. Lade's Single Hardening Model

Lade's model is an elastoplastic model with a single yield surface which expressed in terms of stress invariants. The hardening parameter in this model is assumed to be the total plastic work,

which is used to define the evolution of the yield surface. Compared to the modified Cam clay model and Drucker-Prager model, this model involves 11 parameters that can be determined from three CD triaxial compression tests and one isotropic compression test.

2.3. Elastic Viscoplastic Models

It is essential to use a constitutive model that account for time dependency of the stress–strain–strength properties of soils to obtain realistic solutions for time-dependent engineering problems which considering viscoplastic behavior of soil.

2.3.1. Hypothesizes

In terms of the calculations based on the assumption of creep starts at the beginning of the loading, there are two hypothesize:

Hypothesize 1:

Consolidation includes primary consolidation and secondary consolidation. For the hypothesize 1, Yin and Graham (1994) proposed that primary consolidation occurs because of the changes in pore water pressure (hydraulic gradients), however, the 'secondary compression' is due to creep (viscosity) of clay structures. This hypothesize is supported by Terzaghi's 1-D consolidation theory.

In the Terzaghi's 1-D consolidation theory, he assumes that the relationship between effective stress and void ratio is independent of time and that changes in void ratio is because of the changes in excess pore water pressures (Mesri et al. 1973). In some special cases, the creep deformation is insignificant during primary consolidation, and is assumed to start at the end of primary consolidation.

However, in the general case, the total deformation results from a coupled process involving both mechanical loading and viscous (creep) effects. Creep deformation should be assumed to commence at the start of the loading (Wong et al. 2018).

Hypothesize 2:

Hypothesis 2 assumes that creep (viscous) behavior occurs during the whole consolidation process. Given that primary consolidation consists of a creep deformation, which is increasing with time, the value of eEOP (void ratio at the end of primary consolidation) for thin and thick soil samples should be based on the results of this assumption (Azari et al. 2014).

Hypothesize 2 is consistent with approaches adopted in rheology and viscoplastic theories and used in continuum mechanics (Yin and Graham 1994).

2.3.2. Semilogarithmic Creep Law

In order to analyze the creep behavior on the soil, it is necessary to establish some creep laws. Semilogarithmic creep law is convenient to plot the secondary compression against the logarithm of time to describe the magnitude the creep strains in the odometer tests (Azari et al. 2014).

However, there are some limits for this creep law. Firstly, the coefficient of secondary compression is assumed equal for one specific soil. It is an oversimplification of the volumetric confined creep of any soil, because there are a lot of factors (e.g, time and the applied vertical stress) which may have effects on the results. What's more, logarithmic law is strictly valid only for conditions that are identical to those of the tests from which they have been derived, for example, one-dimensional conditions, the strains tend toward infinity when time tends toward infinity, and so the logarithmic law may overestimate the long-term creep settlements.

This implies that any application of the expressions requires the definition of an origin for the time scale. To overcome the limitations of the logarithmic law, Suklje (1957) introduce a strain-rate approach which identified a unique relationship between the current state of effective vertical stress and strain for a given constant strain rate, in other words, the isotach concept. There is an example using the isotach concept in the Figure 2-1.

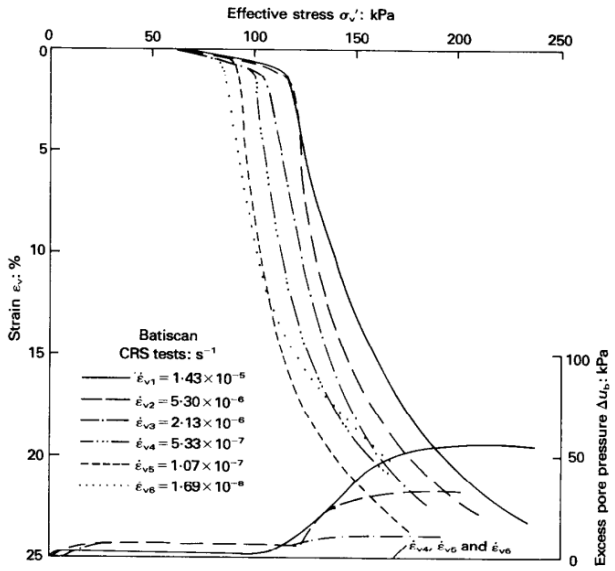

Figure 2-1 Typical CRS oedometer tests on Batisean day, from Leroueil et al. (1985).

2.3.3. Perzyna Viscoplastic Model

Perzyna (1963) proposed some models based on the elastic viscoplastic (EVP) modelling framework, in which total strain rates were divided into elastic strain rate and visco-plastic strain rate components, under the conditions of tri-axial stress states and generalized stress states. His original framework is also known as overstress viscoplasticity. A change of stress within the yield surface ($F \leq 0$) causes time-independent elastic deformations, on the other side, a change of stress resulting in a position outside the yield surface ($F > 0$) results in time-dependent plastic deformations in addition to the elastic deformations (Kurz 2014).

The original model for describing the elastic viscoplastic behavior established by Perzyna (1963) has provided a foundation. Several models have been developed using this framework, for example, the Adachi/Okano model (Adachi and Okano 1974), the Katona model (Katona and Mulert 1984), the Prisco model (di Prisco and Imposimato 1996), the Oka model (Oka 1988), the Zienkiewicz model (Al-Darzi et al. 1989), the Akai model (Goodman 1974), and the Desai model (Desai and Zhang 1987).

2.3.4. Bjerrum's assumption

Bjerrum (1967) defines the 'instant' and 'delayed' compression and he has provided a time line model aimed at improving the understanding of the time-dependent stress-strain behavior on consolidation, as shown in Figure 2-2. The time lines always begin with an 'instant' time line to describe first-time compression (lowest value of e for a given initial load), which can be determined as a 1-day time line by applied stress increments at intervals of 24 h, or by interpretation of other loading intervals in classical odometer tests (Kurz 2014). He also proposed that the delayed compression could be described by parallel lines in a diagram which represents a series of equilibrium relationships after different periods of sustained loading.

Another key feature of Bjerrum's model is that the model considered the observed overconsolidation of aged normally consolidated natural clays (Liingaard et al. 2004).

However, there is also some limitations in the Bjerrum's model. Firstly, Bjerrum's understanding of the 'instant time line' was flawed and in conflict with observations of high constant rate of strain tests. Secondly, the 'instant time line' should be associated with the κ-line, not the λ-line. Thirdly, Yin (1990) questions that Bjerrum's time lines were obtained from single-stage consolidation tests and that the method for finding 'equivalent time' is ill-defined.

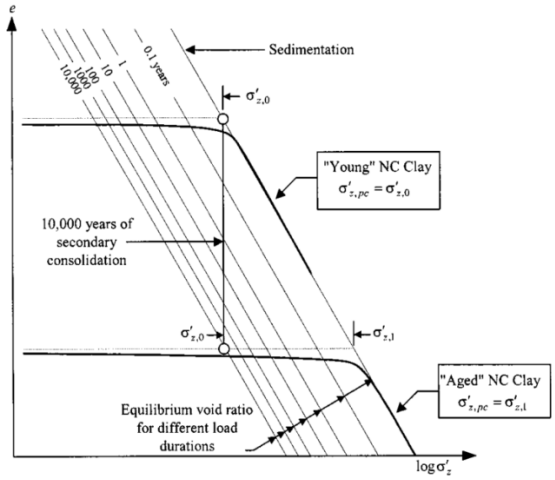

Figure 2-2 Geological history and compressibility of a young and an aged normally consolidated clay, from Liingaard et al. (2004).

2.3.5. Singh-Mitchell Model

Sing and Mitchell (1968) supposed a simple three-parameter phenomenological equation that may be used to describe the strain-rate–time relation of clayey soils when subjected to constant stress, which was based on the analysis of drained and undrained triaxial creep tests on several of clays. He observed a general relationship between the logarithm of the axial strain rate and the logarithm of time, irrespective of whether the strain versus logarithm of time is linear or nonlinear, as shown in Figure 2-3. The Singh and Mitchell model can describe either fading creep or nonfading creep.

But the Singh and Mitchell's creep model has some limitations: (1) the model can't describe the creep behavior at a constant level of stress in three-dimensional conditions and the model is only valid for first time loading; (2) for a particular soil, m is assumed to be constant in the model. However, other creep curves at different stress levels may involve different values of m for the same soil (Augustesen et al. 2004).

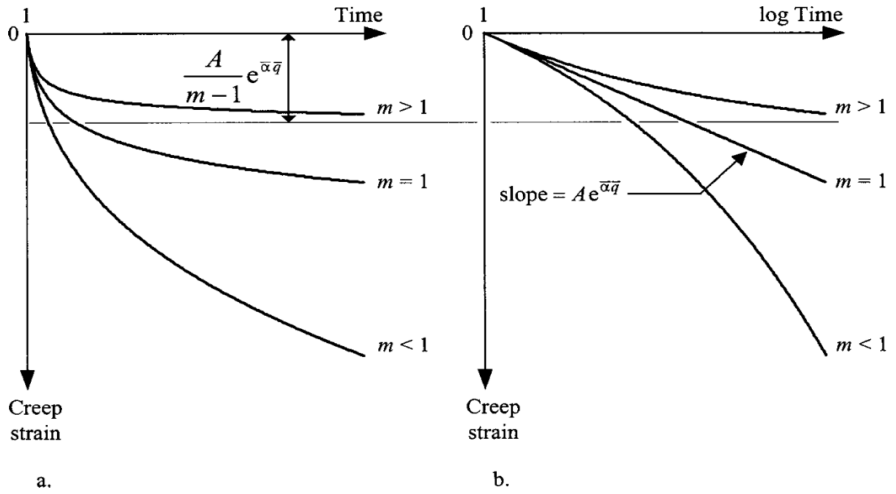

Figure 2-3 Creep curves predicted by the stress–strain–time functions, from Liingaard et al. (2004).

2.3.6. Tavenas Model

Tavenas et al. (1978) held that creep deformations can be broken into volumetric and shear components. The development with time of both volumetric and shear strains can be represented by a phenomenological equation which was proposed by Singh and Mitchell in 1968. The stress function in the equation not only needs to be defined separately for each strain component, but also needs to be defined by reference to the limit state of the clay.

Therefore, Tavenas (1977) proposed a qualitative model (YLIGHT) of the clay behavior which was developed on the basis of the limit state concept to observe the relationship between stress, strain and time. This model, which not only integrates time effects, pointed out the necessity of a stringent consideration of the actual effective stress conditions in the analysis of time dependent phenomena, but also clearly indicated that a distinction between strength and deformation problems.

2.3.7. Leroueil Framework

Leroueil et al. (1985) investigated the isotach concept by using multiple stage loading tests, constant rate of strain tests, controlled hydraulic gradient tests, and long-term creep tests on several soils and confirmed the model which provided by Suklje (1957). Their investigation shows the soil sample clearly followed a unique compression curve under a constant strain rate until the strain rate was changed again (Figure 2-4).

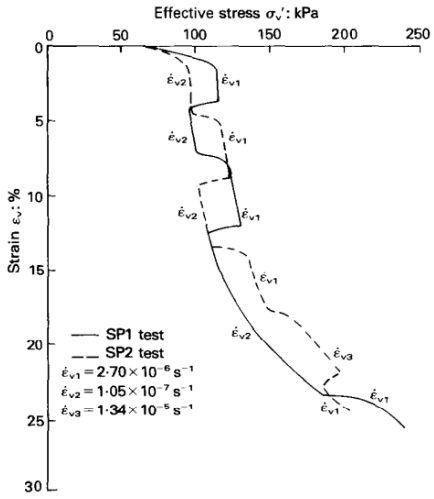

Figure 2-4 Special CRS oedometer tests on Batiscan clay, from Leroueil et al. (1985).

And they suggested that relationship between the effective stress rate, stress and strain could be described completely by two equations, one giving the variation of the pre-consolidation pressure with the strain rate, as shown in equation (2.1):

$$P_c = f(\dot{\varepsilon}_v) \tag{2.1}$$

And another equation presents the normalized effective stress–strain relation:

$$\frac{\sigma'}{P_c} = g(\varepsilon_v) \tag{2.2}$$

The results from CRS oedometer tests on Batiscan can prove the above equations, as shown in Figures 2-5 and 2-6.

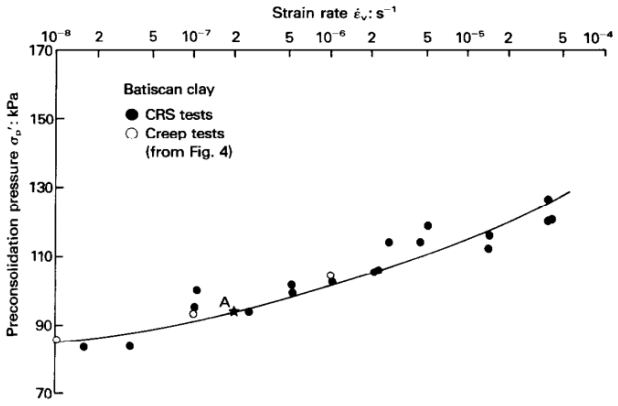

Figure 2-5 Variation in pre-consolidation pressure with strain rate for Batiscan clay, from Leroueil et al. (1985).

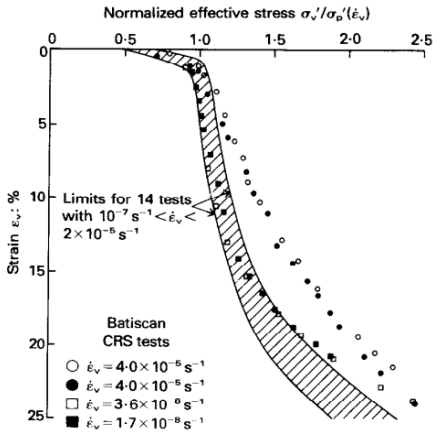

Figure 2-6 Normalized effective stress-strain relationship, from Leroueil et al. (1985).

When the two relationships are known for a given soil, any stress–strain–strain rate relationship for the soil could easily be reconstructed and the viscous properties of the clay are directly related to the primary deformation properties.

However, for the Leroueil's framework, the concept is developed mainly from observations in the normally consolidated range, so gives poor predictions in the heavily reconsolidated range where the elastic strains are relatively significant.

2.3.8. Yin and Gracham model

Yin and Graham (1989) pointed out that the time line which was proposed by Bjerrum for considering creep compression under 1D straining should be a line with a carefully defined "equivalent time," not the ordinary duration of loading.

They defined equivalent time and other concepts such as "instant time" lines and "reference time" lines for 1D applications, as shown in Figure 2-7. The concept of ''equivalent time,' which is used to model creep behavior of normally consolidated and reconsolidated clays, as a function of the effective stress, stress and strain to predict in a variety of test conditions, e.g., relaxation tests, tests with a constant rate of strain or constant rate of stress. Compared to Bjerrum's model and the strain-rate approach, it is emphasized that the ability to model the difference between NC and overconsolidation ratio (OCR) clays and relaxation.

After framing these concepts in terms of logarithmic functions, they derived a general 1D EVP constitutive model for time-dependent stress–strain behavior of clays. The predictions of the one-dimensional viscous behavior, for example, creep and strain rate effects are generally in good agreement with experiments on soft soils. The best agreements are obtained by the use of the power function approach is because that improved options for calibrating the model as compared with the logarithmic model.

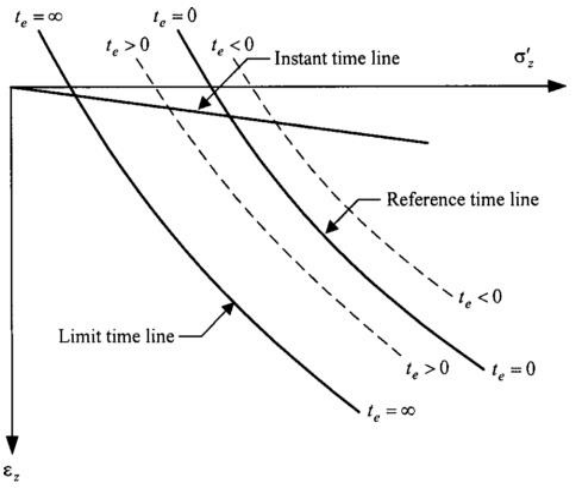

Figure 2-7 Illustration of instant time line, reference time line, limit time line, and time lines for positive and negative equivalent times, from Liingaard et al. (2004).

3. Drucker-Prager/Cap model and Singh-Mitchell model

3.1. General introduction

The general understanding of the soil behavior has increased progressively over the last decades. However, deposits of soft clays may still be considered as a research subject and may lead to huge geotechnical challenges (Bjerre 2015).

Constitutive models that relate stresses and strains must be established in order to predict the material behavior. Several material models aiming to increase the accuracy when predicting the stress-strain relationship of real materials have been developed over the last decades. Therefore, to develop a viscoplastic model, it is necessary to have a basic understanding of the general elastic-plastic theory and the continuum mechanics behind constitutive models (Bjerre 2015).

3.2. Stress and strain

Principal stresses represent a stress situation where stresses acting perpendicular to the plane without any shear stresses. It is possible to determine the principle stresses by use of Cauchy's law through an Eigenvalue problem:

$$\left(\sigma - \sigma' I\right) n = 0 \tag{3.1}$$

$$\left(\sigma_{ij}' + \sigma' \delta_{ij}\right) n = 0 \tag{3.1.a}$$

Where $\delta_{ij} = \begin{cases} 1, i = j \\ 0, i \neq j \end{cases}$, I is the identity matrix and n is a normal vector.

$$I_1 = \sigma_1' + \sigma_2' + \sigma_3' \tag{3.1.b}$$

$$I_2 = -\sigma_1^{'}\sigma_2^{'} - \sigma_1^{'}\sigma_3^{'} - \sigma_2^{'}\sigma_3^{'} \tag{3.1.c}$$

$$I_3 = \sigma_1^{'}\sigma_2^{'}\sigma_3^{'} \tag{3.1.d}$$

The deviatoric stress is defined as:

$$s = \sigma - p \tag{3.2}$$

$$s_{ij} = \left(\sigma^{'}_{ij} - p\delta_{ij}\right) \tag{3.2.a}$$

Where $\delta_{ij} = \begin{cases} 1, i = j \\ 0, i \neq j \end{cases}, i, j = 1, 2, 3$.

where p is the mean stress tensor containing the mean stress in the diagonal. The mean stress is defined by:

$$p = \frac{1}{3}\left(\sigma_{11}^{'} + \sigma_{22}^{'} + \sigma_{33}^{'}\right) = \frac{1}{3}\left(\sigma_1^{'} + \sigma_2^{'} + \sigma_3^{'}\right) = \frac{I_1}{3} \tag{3.2.b}$$

And the Mises stress is given by:

$$q = \sqrt{3 s_{ij} s_{ij} / 2} \tag{3.3}$$

$$\varepsilon = \begin{bmatrix} \varepsilon_{11}, \varepsilon_{12}, \varepsilon_{13} \\ \varepsilon_{21}, \varepsilon_{22}, \varepsilon_{23} \\ \varepsilon_{31}, \varepsilon_{32}, \varepsilon_{33} \end{bmatrix} \tag{3.4}$$

The total stain for a soft clay is given by:

$$d\varepsilon = d\varepsilon^{e} + d\varepsilon^{p} + d\varepsilon^{cr} \tag{3.5}$$

Where $d\varepsilon^e$ is the elastic strain, $d\varepsilon^p$ is the time-independent plastic strain, and $d\varepsilon^{cr}$ is the creep strain.

The volumetric strain is given by:

$$\varepsilon_p = \varepsilon_v = \varepsilon_1 + \varepsilon_2 + \varepsilon_3 \tag{3.6}$$

The deviatoric strain is given by:

$$\varepsilon_q = \frac{\sqrt{2}}{3}\sqrt{(\varepsilon_1 - \varepsilon_2)^2 + (\varepsilon_2 - \varepsilon_3)^2 + (\varepsilon_3 - \varepsilon_1)^2} \tag{3.7}$$

$$\{d\sigma\}^{\mathrm{T}} = \{d\sigma_{11}, d\sigma_{22}, d\sigma_{33}, d\sigma_{12}, d\sigma_{23}, d\sigma_{31}\} \tag{3.8}$$

$$\{d\varepsilon^e\}^{\mathrm{T}} = \{d\varepsilon^e{}_{11}, d\varepsilon^e{}_{22}, d\varepsilon^e{}_{33}, d\gamma^e_{12}, d\gamma^e_{23}, d\gamma^e_{31}\} \tag{3.9}$$

3.3. Elastoplastic theory

The material response is partly reversible and partly irreversible in elasto-plastic theory. Therefore, the strains can be decomposed into recoverable elastic strains ε^e and irrecoverable plastic strains ε^p.

$$d\varepsilon = d\varepsilon^e + d\varepsilon^p \tag{3.10}$$

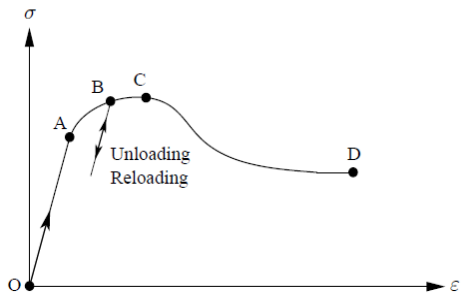

Figure 3-1 Stress-strain path for a real soil, from Bjerre (2015).

Yielding is defined as the transition between the elastic and plastic region, which is shown in the Figure 3-1 (point A).

An elastic-plastic model includes the information of elasticity, plasticity and yielding to predict the relationship between stresses and strains, which can divide into two parts: 1) Stress changes inside the yield surface which are associated by pure elastic strains; 2) Stress changes at the edge of the yield surface which are associated by a combination of elastic and plastic strains.

The flow rule describes the relationship between the plastic strains to the plastic potential, the flow rule includes: 1) associated flow rule; 2) non-associated flow rule.

For the associated flow rule, then the yield and the plastic potential surfaces should have the same shape and size,

$$d\varepsilon^p = d\lambda \frac{\partial Q}{\partial \sigma} = d\lambda \frac{\partial F}{\partial \sigma} \tag{3.11}$$

where F represents the yield surface, Q represents the plastic potential.

For the non-associated flow rule, then the yield and the plastic potential surfaces should not have the same shape and size,

$$d\varepsilon^p = d\lambda \frac{\partial Q}{\partial \sigma} \neq d\lambda \frac{\partial F}{\partial \sigma} \tag{3.12}$$

The hardening rule is associated to the development of plastic strains with respect to the evolution of the yield surface through the plastic multiplier $d\lambda$.

For the given stress state and for any stress state which can be introduced by incremental stresses, the following derivations are applied to derive the plastic multiplier $d\lambda$ based on consistency condition.

$$F(\sigma, \mathrm{H}) = 0 \tag{3.13}$$

$$F(\sigma + d\sigma, \mathrm{H} + dH) = 0 \tag{3.13.a}$$

$$dF = \left\{\frac{\partial F}{\partial \sigma}\right\}^T d\sigma + \left\{\frac{\partial F}{\partial H}\right\} dH = 0 \tag{3.13.b}$$

$$\left\{\frac{\partial F}{\partial \sigma}\right\}^T d\sigma + \frac{\partial F}{\partial H}\left\{\frac{\partial H}{\partial \varepsilon^P}\right\}^T \left\{d\varepsilon^p\right\} = 0 \tag{3.13.c}$$

$$\left\{\frac{\partial F}{\partial \sigma}\right\}^T d\sigma + \frac{\partial F}{\partial H}\left\{\frac{\partial H}{\partial \varepsilon^P}\right\}^T d\lambda \left\{\frac{\partial g}{\partial \sigma}\right\} = 0 \tag{3.13.d}$$

Then

$$d\lambda = -\frac{\left\{\frac{\partial F}{\partial \sigma}\right\}^T d\sigma}{\frac{\partial F}{\partial H}\left\{\frac{\partial H}{\partial \varepsilon^P}\right\}^T \left\{\frac{\partial g}{\partial \sigma}\right\}} \tag{3.13.e}$$

Assume

$$A = -\frac{\partial F}{\partial H}\left\{\frac{\partial H}{\partial \varepsilon^P}\right\}^T \left\{\frac{\partial g}{\partial \sigma}\right\} \tag{3.13.f}$$

Then

$$d\lambda = \frac{\left\{\frac{\partial F}{\partial \sigma}\right\}^T d\sigma}{A} \tag{3.13.g}$$

3.4. Modified Drucker-Prager/Cap model

In this research, Drucker-Prager/Cap model was used to perform constitutive modelling on stress-strain relations of soft clays considering the viscoplastic behavior.

The computer simulation of the compaction behavior of particulate materials (e.g., ceramic, metal, pharmaceutical powders and soils) has received much interest for decades. Beside the shear yielding (failure) behavior, particulate materials exhibit hydrostatic pressure-dependent yielding behavior, however, the yielding of bulk metals do not exhibit the hydrostatic pressure dependency. The modified Drucker–Prager cap (MDPC) constitutive model has been frequently employed in many engineering areas to describe such yielding behavior of particulate materials (Shin et al. 2015).

Compared to the original Drucker – Prager model, the modified Drucker – Prager model adds a cap yield surface. The cap surface serves two main purposes: firstly it bounds the yield surface in hydrostatic compression, therefore providing an inelastic hardening mechanism to represent plastic compaction; secondly, it helps control volume dilatancy when the material yields in shear by providing softening as a function of the inelastic volume increase created as the material yields on the Drucker – Prager shear failure and transition yield surfaces. The model uses associated flow in the cap region and a particular choice of nonassociated flow in the shear failure and transition regions (Abaqus 2016).

The modified Drucker–Prager/cap plasticity model yield surface consists of three parts: a Drucker–Prager shear failure surface, an elliptical *cap*, and a smooth transition region between the shear failure surface and the cap. If we neglect the transition region between the shear failure surface and the cap, the yield surface is shown in Figure 3-2.

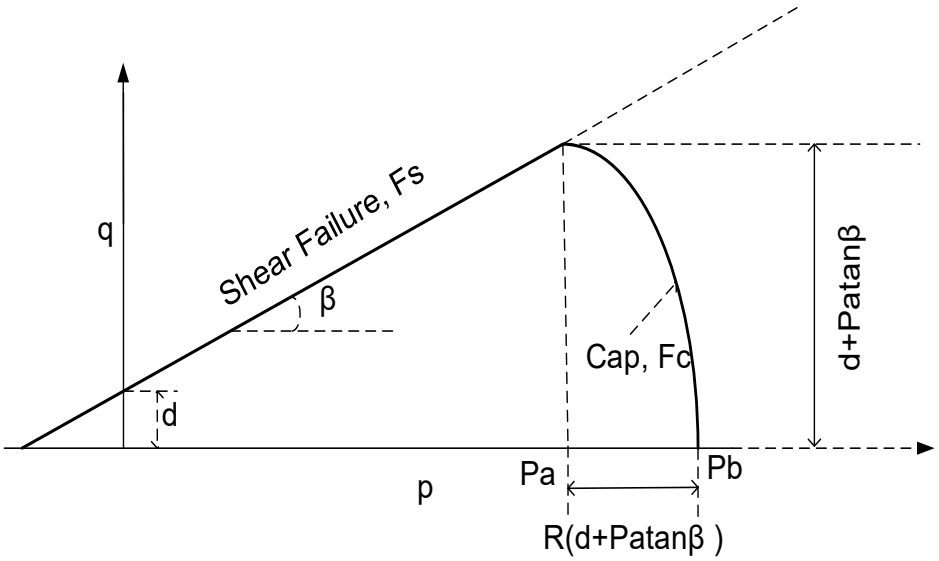

Figure 3-2 Yield surfaces of the modified cap model in the meridional (p–q) plane, after Abaqus (2016).

The Drucker-Prager failure surface and the cap yield surface determine the shear and consolidation yielding, respectively. When the stress state causes yielding on the Drucker – Prager shear failure surface, the soil is treated as perfect plastic material where shear hardening is not considered in this study. Failure and plastic potential functions for time-independent plastic behaviors are shown in Table 3-1.

Table 3-1 Failure and plastic potential functions for the time-independent plastic behavior.

Functions	Descriptions
$f_s^p = q - p\tan\beta - d$	Failure function for shear
$f_c^p = \sqrt{(p-p_a)^2 + (Rq)^2} - R(d + p_a\tan\beta)$	Failure function for cap-hardening
$g_s^p = \sqrt{\left[(p_a - p)\tan\beta\right]^2 + q^2}$	Plastic potential for shear
$g_c^p = \sqrt{(p-p_a)^2 + R^2q^2}$	Plastic potential for cap-hardening

Elastic behavior is considered as linear elastic which uses the generalized Hooke's law. Alternatively, in order to calculate the elastic strains, an elasticity model in which the bulk elastic stiffness increases when the material undergoes compression.

The onset of plastic behavior is determined by the Drucker–Prager failure surface and the cap yield surface. The cap yield surface, which is an ellipse with eccentricity = R in the p–t plane. The cap surface hardens or softens can be considered as a function of the volumetric plastic strain. R is a material parameter that controls the shape of the cap and α is a small number (typically, 0.01 to 0.05) which is used to define a smooth transition surface between the Drucker–Prager shear failure surface and cap surface (Abaqus 2016).

For the deviatoric plane, as shown in Figure 3-3, the cap yield surface is dependent on the third stress invariant, *r*. The cap surface hardens (expands) or softens (shrinks) as a function of the volumetric plastic strain. When the stress state causes yielding on the cap, volumetric plastic strain (compaction) results cause the cap to expand (hardening). But when the stress state causes yielding on the Drucker–Prager shear failure surface, volumetric plastic dilation results, which causing the cap to shrink (softening) (Abaqus 2016).

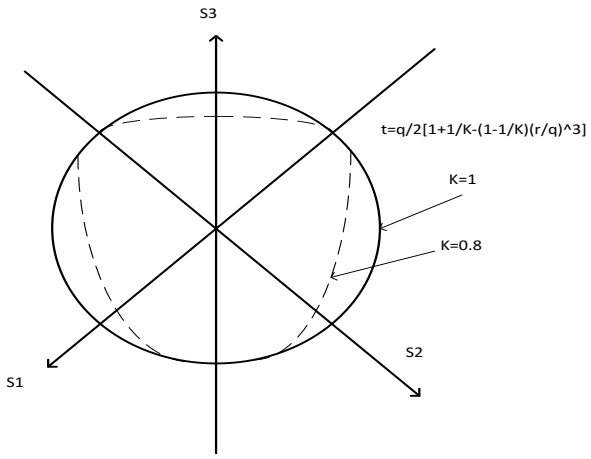

Figure 3-3 Projection of the modified cap yield/flow surfaces, after Abaqus (2016).

In Abaqus, the deviatoric stress is defined as:

$$t = \frac{q}{2}\left[1+\frac{1}{K}-(1-\frac{1}{K})\left(\frac{r}{q}\right)^3\right] \tag{3.14}$$

Where K is the parameter, which controls the shape of yielding surface in the deviatoric plane (π plane) and r is the third invariant of deviatoric stress. In this research, a value of 1 is used for K, so $t = q$.

In the Drucker-Prager/Cap model, the flow potential surface in the *p*–*t* plane consists of two parts, as shown in Figure 3-4. In the cap region, the shape of the plastic flow is identical to the

yield surface (i.e., associated flow). For the Drucker–Prager failure surface and the transition yield surface, a nonassociated flow is assumed: the shape of the flow potential in the *p*–*t* plane is different from the yield surface. As shown in Figure 3-4, the two elliptical portions, *Gc* and *Gs*, which provide a continuous potential surface. The material stiffness matrix is not symmetric because of the non-associated flow used in this model.

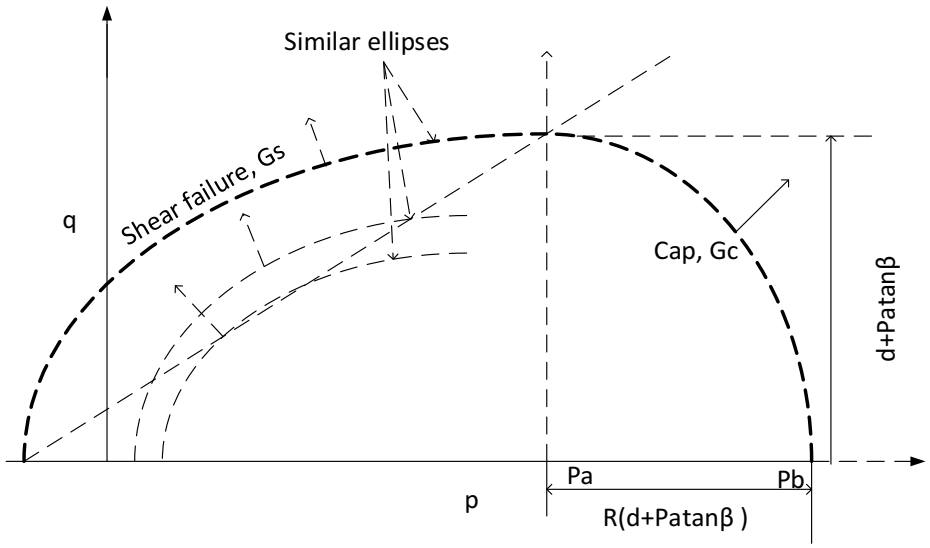

Figure 3-4 Flow potential of the modified cap model in the p–t plane, after Abaqus (2016).

The relationship between soil friction angle, ϕ', cohesion strength *c*, and Drucker-Prager parameters can be found from:

$$\begin{cases} d = \dfrac{18c\cos\phi'}{3-\sin\phi'} \\ \tan\beta = \dfrac{6\sin\phi'}{3-\sin\phi'} \end{cases} \tag{3.15}$$

The hydrostatic compression yield stress p_b is a function of volumetric inelastic strain ε_v^p (time independent plastic + creep). The strain hardening law used for the cap hardening has the form of:

$$dp_b = p_b \left(\frac{1+e_0}{\lambda_c - k} \right) d\varepsilon_v^p \tag{3.16}$$

Where λ_c and k are the compression and rebound indices. e_0 is the initial void ratio.

The hardening–softening behavior is simply described by a piecewise linear function relating the mean effective (yield) stress P_b and the volumetric plastic strain as shown in Figure 3-5.

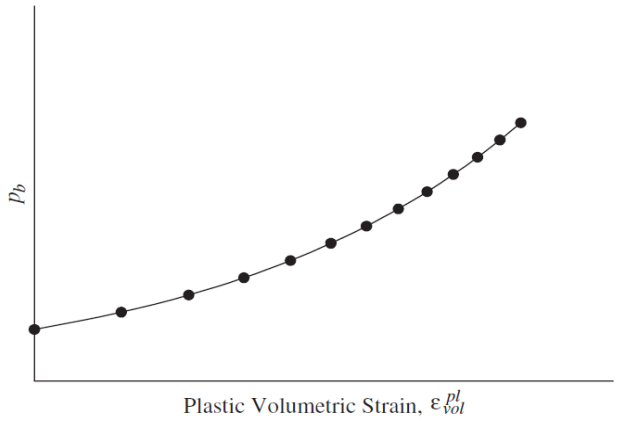

Figure 3-5 Typical cap hardening behavior, from Abaqus (2016).

P_a is an evolution parameter which controls the hardening–softening behavior as a function of the volumetric plastic strain. P_a can be derived from:

$$p_a = \frac{p_b - Rd}{1 + R\tan\beta} \tag{3.17}$$

The elastoplastic stiffness matrix, $[D]_{ep}$, can be derived from the following euqations:

$$\{d\varepsilon\} = \{d\varepsilon^e\} + \{d\varepsilon^p\} \tag{3.18}$$

$$[D]\{d\varepsilon\} = [D]\{d\varepsilon^e\} + [D]\{d\varepsilon^p\} \tag{3.18.a}$$

$$[D]\{d\varepsilon\} = \{d\sigma\} + [D]d\lambda\left\{\frac{\partial g}{\partial \sigma}\right\} \tag{3.18.b}$$

$$\frac{1}{A}\left\{\frac{\partial F}{\partial \sigma}\right\}^T d\sigma = \frac{1}{A}\left\{\frac{\partial F}{\partial \sigma}\right\}^T \left([D]\{d\varepsilon\} - [D]d\lambda\left\{\frac{\partial g}{\partial \sigma}\right\}\right) \tag{3.18.c}$$

$$d\lambda = \frac{1}{A}\left\{\frac{\partial F}{\partial \sigma}\right\}^T \left([D]\{d\varepsilon\} - [D]d\lambda\left\{\frac{\partial g}{\partial \sigma}\right\}\right) \tag{3.18.d}$$

$$d\lambda = \frac{\left\{\frac{\partial F}{\partial \sigma}\right\}^T [D]}{A + \left\{\frac{\partial F}{\partial \sigma}\right\}^T [D]\left\{\frac{\partial g}{\partial \sigma}\right\}}\{d\varepsilon\} \tag{3.18.e}$$

$$\{d\sigma\} = \left\{[D] - \frac{[D]\frac{\partial g}{\partial \sigma}\left\{\frac{\partial F}{\partial \sigma}\right\}^T [D]}{A + \left\{\frac{\partial F}{\partial \sigma}\right\}^T [D]\left\{\frac{\partial g}{\partial \sigma}\right\}}\right\}\{d\varepsilon\} \tag{3.18.f}$$

$$[D]_{ep} = D - \frac{[D]\frac{\partial g}{\partial \sigma}\left\{\frac{\partial F}{\partial \sigma}\right\}^T [D]}{A + \left\{\frac{\partial F}{\partial \sigma}\right\}^T [D]\left\{\frac{\partial g}{\partial \sigma}\right\}} \tag{3.18.g}$$

For shear yielding

The shear hardening is not considered in this study, so there is no elastoplastic stiffness matrix. Before failure, elastic matrix will be used to calculate the stress increment. When the failure function was satisfied, all the given strain (strain control approach) is the plastic strain. For triaxial test condition, axial strain is given, the radial strain component should be back calculated using the flow rule.

$$d\varepsilon^p = \chi \frac{\partial g_s^p}{\partial \sigma} \tag{3.19}$$

$$\frac{\partial g_s^p}{\partial \sigma} = -\frac{(p_a - p)(\tan\beta)^2}{\sqrt{\left[(p_a - p)\tan\beta\right]^2 + q^2}} \cdot \frac{1}{3}\mathbf{I} + \frac{q}{\sqrt{\left[(p_a - p)\tan\beta\right]^2 + q^2}}\mathbf{n} \tag{3.19.a}$$

where $\mathbf{n} = \frac{\partial q}{\partial \sigma} = \frac{3}{2}\frac{\mathbf{s}}{q}$, and $\mathbf{I}$ is the unit vector

For cap hardening

The elastoplastic stiffness matrix is given by:

$$[D]_{ep} = [D] - \frac{[D]\left\{\frac{\partial g_c^p}{\partial \sigma}\right\}\left\{\frac{\partial f_c^p}{\partial \sigma}\right\}^T [D]}{A^* + \left\{\frac{\partial f_c^p}{\partial \sigma}\right\}^T [D]\left\{\frac{\partial g_c^p}{\partial \sigma}\right\}} \tag{3.20}$$

Where

$$\frac{\partial f_c^p}{\partial \sigma} = \frac{R^2 q}{\sqrt{(p - p_a)^2 + (Rq)^2}}\mathbf{n} + \frac{p - p_a}{\sqrt{(p - p_a)^2 + (Rq)^2}}\frac{1}{3}\mathbf{I} \tag{3.20.a}$$

$$\frac{\partial g_c^p}{\partial \sigma} = \frac{R^2 q}{\sqrt{\left(p - p_a\right)^2 + \left(Rq\right)^2}}\mathbf{n} + \frac{\left(p - p_a\right)}{\sqrt{\left(p - p_a\right)^2 + \left(Rq\right)^2}}\frac{1}{3}\mathbf{I} \tag{3.20.b}$$

$$A^* = (-)\frac{\partial f_c^p}{\partial p_b}\frac{\partial p_b}{\partial \varepsilon_v^p}\frac{\partial g_c^p}{\partial p} \tag{3.20.c}$$

$$\frac{\partial p_b}{\partial \varepsilon_v^p} = p_b\left(\frac{1+e_0}{\lambda_c - k}\right) \tag{3.20.d}$$

$$\frac{\partial f_c^p}{\partial p_b} = \frac{\partial f_c^p}{\partial p_a}\frac{\partial p_a}{\partial p_b} \tag{3.20.e}$$

$$\frac{\partial p_a}{\partial p_b} = \frac{1}{1 + R\tan\beta} \tag{3.20.f}$$

$$\frac{\partial f_c^p}{\partial p_a} = \frac{-\left(p - p_a\right)}{\sqrt{\left(p - p_a\right)^2 + \left(Rq\right)^2}} - R\tan\beta \tag{3.20.g}$$

$$\frac{\partial g_c^p}{\partial p} = \frac{p - p_a}{\sqrt{\left(p - p_a\right)^2 + \left(Rq\right)^2}} \tag{3.20.h}$$

3.5. Singh-Mitchell model

In Singh-Mitchell model, there are two separate and independent creep mechanisms. One is a shear mechanism ($d\varepsilon_s^{cr}$), and the other is a consolidation mechanism ($d\varepsilon_c^{cr}$). The total creep strain is a combination of those two components:

$$d\varepsilon^{cr} = d\varepsilon_s^{cr} + d\varepsilon_c^{cr} \tag{3.21}$$

The regions of activity of shear and consolidation creep mechanisms are illustrated in Figure 3-6.

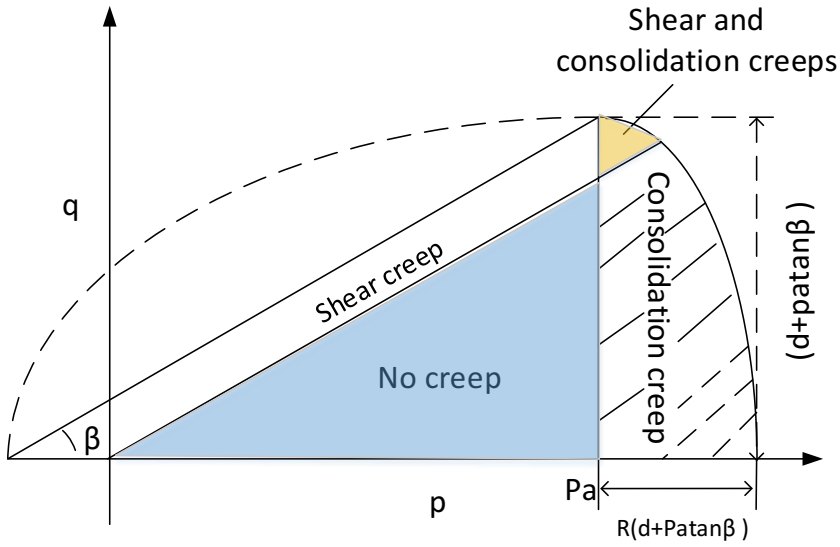

Figure 3-6 Regions of activity of shear and consolidation creep mechanisms, after Abaqus (2016).

The Singh-Mitchell creep model for shear creep takes the form as:

$$\dot{\varepsilon}_{11} = A^s e^{\alpha^s \sigma_{cr}^s} \left(\frac{t_1}{t} \right)^{m^s} \tag{3.22}$$

where A^s, α^s, and m^s are three creep parameters which should be derived from creep or relaxation tests results; t_1 is the initial time, normally a unit value of 1 is used.

The Singh-Mitchell creep model for consolidation creep takes the form as:

$$\dot{\varepsilon}_v = A^c e^{\alpha^c \sigma_{cr}^c} \left(\frac{t_1}{t} \right)^{m^c} \tag{3.23}$$

The shear mechanism is active for all stress states that have a positive equivalent creep stress as explained below. The consolidation mechanism is active for all stress states in which the pressure is larger than p_a.

For shear creep, the equivalent creep stress, σ_{cr}^{s} is determined as the intersection of the equivalent creep surface with the uniaxial compression curve (Figure. 3-7).

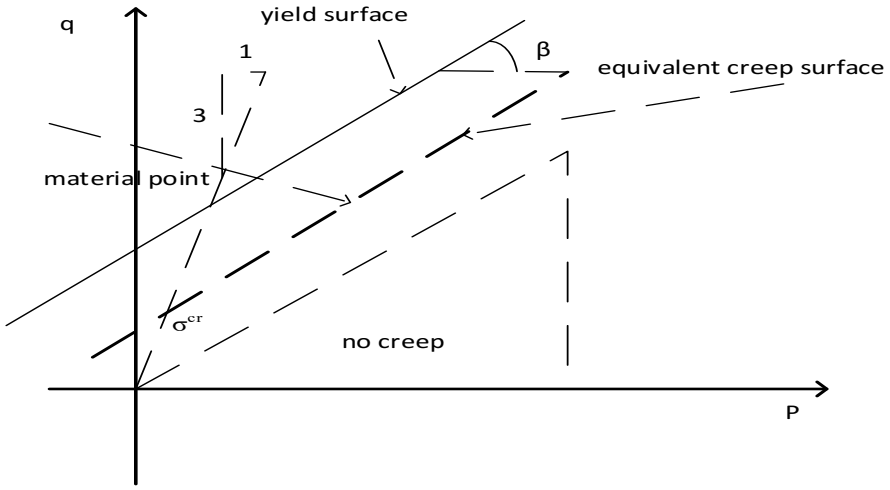

Figure 3-7 Equivalent creep stress for shear creep, after Abaqus (2016).

For consolidation creep, σ_{cr}^{c} is derived from the mean stress p. The equations for calculating σ_{cr} and the function expressions are included are included in Table 3-2.

Table 3-2 Equivalent creep stresses and plastic potential functions for creep behavior.

	Equivalent creep stress	Creep potentials
Shear creep	$\sigma_{cr}^{s}=\dfrac{q-p\tan\beta}{\left(1-\frac{1}{3}\tan\beta\right)}$	$g_{s}^{cr}=\sqrt{\left(0.1\dfrac{d}{(1-\frac{1}{3}\tan\beta)}\tan\beta\right)^{2}+q^{2}}-p\tan\beta$
Consolidation creep	$\sigma_{cr}^{c}=p-p_{a}$	$g_{c}^{cr}=\sqrt{(p-p_{a})^{2}+R^{2}q^{2}}$

The creep potentials in the p–t(q) plane for both mechanisms are shown in Figures. 3-8 and 3-9.

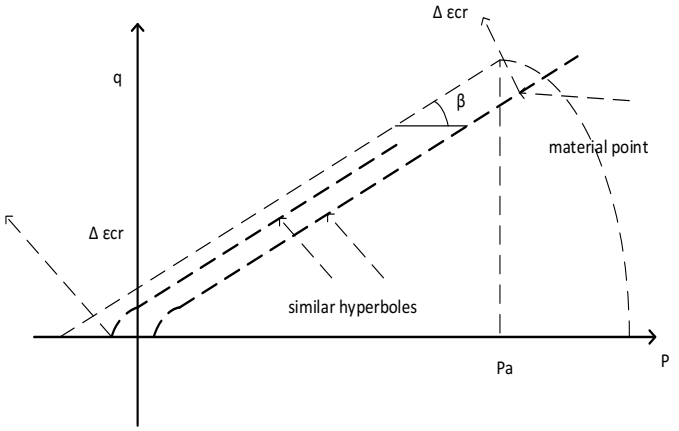

Figure 3-8 Creep potentials: shear mechanism, after Abaqus (2016).

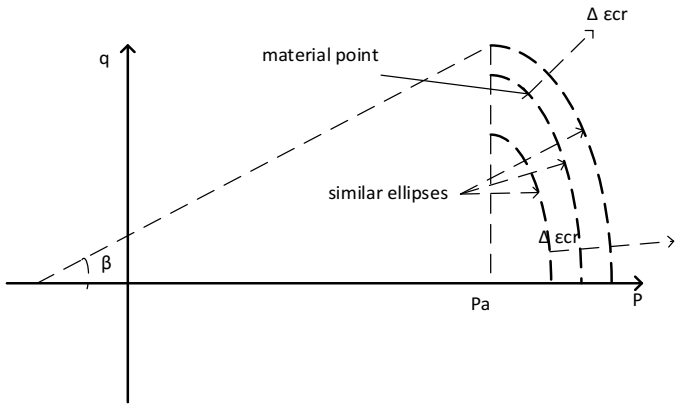

Figure 3-9 Creep potentials: consolidation mechanism, after Abaqus (2016).

In Abaqus, the creep strain rate can be derived from the creep flow rule (the strain rate is given at a unit time interval $\Delta t = 1$ so $d\varepsilon^{cr}$ was used):

$$d\varepsilon^{cr} = \frac{d\bar{\varepsilon}^{cr}}{F^{cr}} \frac{\partial g^{cr}}{\partial \sigma} \tag{3.24}$$

$$F^{cr} = \frac{1}{\bar{\sigma}^{cr}} \sigma : \frac{\partial g^{cr}}{\partial \sigma} \tag{3.24.a}$$

The complicated expression is actually the same with conventional flow rule for creep strain rate, which is similar as the scale function used by Yin and Graham (1999).

$$d\varepsilon^{cr} = \Lambda \frac{\partial g^{cr}}{\partial \sigma} \tag{3.25}$$

Λ can be derived based on lab data.

For uniaxial compression (dominated by shear creep):

$$d\varepsilon_{11}^{cr} = \Lambda^{s} \frac{\partial g_s^{cr}}{\partial \sigma^{cr}} \tag{3.26}$$

$$\Lambda^{s} = \frac{d\varepsilon_{11}^{cr}}{\partial g_s^{cr} \Big/ \partial \sigma^{cr}} \tag{3.26.a}$$

$$\sigma^{cr} = q = \sigma_{11} \tag{3.26.b}$$

$$\frac{\partial g_s^{cr}}{\partial \sigma_{11}} = \frac{\sigma_{11}}{\sqrt{\left(0.1 \frac{d}{(1-\frac{1}{3}\tan\beta)} \tan\beta\right)^2 + {\sigma_{11}}^2}} - \frac{1}{3}\tan\beta \tag{3.26.c}$$

Thus the shear creep can be calculated from

$$d\varepsilon_{s}^{cr} = \Lambda^{s} \frac{\partial g_s^{cr}}{\partial \sigma} \tag{3.27}$$

$$\frac{\partial g_s^{cr}}{\partial \sigma} = \frac{q}{\sqrt{\left(0.1\frac{d}{(1-\frac{1}{3}\tan\beta)}\tan\beta\right)^2 + q^2}}\mathbf{n} - \frac{1}{3}\tan\beta\mathbf{I} \tag{3.27.a}$$

Where $\mathbf{n} = \frac{\partial q}{\partial \sigma} = \frac{3}{2}\frac{\mathbf{s}}{q}$, and $\mathbf{I}$ is the unit vector.

For volumetric compression (dominated by consolidation creep):

$$d\varepsilon_v^{cr} = \Lambda^c \frac{\partial g_c^{cr}}{\partial \sigma^{cr}} \tag{3.28}$$

$$\Lambda^c = \frac{d\varepsilon_v^{cr}}{\partial g_c^{cr} \Big/ \partial \sigma^{cr}} \tag{3.28.a}$$

$$\sigma^{cr} = p - p_a, q = 0 \tag{3.28.b}$$

$$\frac{\partial g_c^{cr}}{\partial \sigma^{cr}} = 1 \tag{3.28.c}$$

So $\Lambda^c = d\varepsilon_v^{cr}$

Thus the consolidation creep can be calculated from

$$d\varepsilon_c^{cr} = \Lambda^c \frac{\partial g_c^{cr}}{\partial \sigma} \tag{3.29}$$

$$\frac{\partial g_c^{cr}}{\partial \sigma} = \frac{1}{\sqrt{(p-p_a)^2 + R^2 q^2}}\left(R^2 q\mathbf{n} + \frac{1}{3}(p-p_a)\mathbf{I}\right) \tag{3.29.a}$$

Theories described in this chapter will be used for proposing a simplified approach of deriving creep parameters to be presented in Chapter 4. The theoretical basis is also critical for the constitutive modeling analysis addressed in Chapters 5 and 6.

4. Deriving creep parameters based on stress relaxation tests

4.1. Introduction

There are six parameters for the shear and consolidation creep models ($A^s, \alpha^s, m^s, A^c, \alpha^c, m^c$). Usually, a large quantity of time-consuming creep tests is required to derive the creep parameters. By contrast, the first three parameters (A^s, α^s, m^s) and the last three parameters (A^c, α^c, m^c) can be estimated from triaxial relaxation tests, where both consolidation plastic strain and shear plastic strain will be generated. In this chapter, an innovative approach based on stress relaxation tests to obtain those creep parameters will be presented. Compared to creep tests, relaxation tests take much less time.

4.2. Consolidation creep parameters

For the consolidation creep parameters, we can obtain parameters by performing stress relaxation test using an oedometer test facility. For the oedometer test, the change in consolidation creep stress is equivalent to the change in the vertical stress:

$$\Delta\sigma_{cr}^{c} = \Delta\sigma_{11} \tag{4.1}$$

During relaxation test, the axial strain component from creep is compensated by the component from linear elastic rebound and expressed as:

$$\int_{t_a}^{t_b} A^c e^{\alpha^c \sigma_{cr}^c} \left(\frac{t_1}{t}\right)^{m^c} dt = \frac{\Delta\sigma_{11}}{E_c} \tag{4.2}$$

Where E_c is the constrained modulus, which is related to Young's modulus E and Poisson's ratio ν from:

$$E_c = \frac{E(1-\nu)}{(1+\nu)(1-2\nu)} \tag{4.3}$$

The creep stress, σ_{cr}^{c} is a function of time, which can be derived using curve fitting based on laboratory measurement on stress time relation. The decreasing trend of σ_{cr}^{c} with the increase of time can be modeled by a simple function as:

$$\sigma_{cr}^{c}(t) = \frac{a}{t+b} \tag{4.4}$$

In order to figure out A^c , α^c and m^c , a derivative free method was used in MATLAB by analyzing the relaxation test data.

There is no analytical solution for $\int_{t_a}^{t_b} Ae^{\alpha\sigma_{cr}} \left(\frac{t_1}{t}\right)^m dt$, so a special numerical algorithm is used to figure out parameters A, α, and m.

Basically, a trial and error approach is applied to solve the problem by finding the proper A, α, and m to have the minimum value of the optimization function, Φ

$$\Phi = \sum_{i=1}^{n} \left(\int_{t_a}^{t_b} Ae^{\alpha\sigma_{cr}^{i}} \left(\frac{t_1}{t}\right)^m dt - \frac{\Delta\sigma_{11}^{i}}{E} \right)^2 \tag{4.5}$$

where *i* indicates for the relaxation stage number. When there are three stages of relaxation tests, n=3. The MATLAB optimization tool box can be applied to conduct nonlinear optimization with multiple variables using the derivative-free method (Conn et al. 2009).

4.3. Shear creep parameters

Similarly, under a triaxial testing condition, the shear creep stress is equivalent to the Mises shear stress and expressed as

$$\sigma_{cr}^{s} = q \tag{4.6}$$

Shown in Figure 3-6, the consolidation creep is usually accompanyed with the shear creep. It is also necessary to divide the total creep strain into consolidation and shear components for total creep strain occuring during the stress relaxation. Figure 4-1 shows the stress path of a relaxation test. During the process of stress relaxation in a triaxial test, the mean stress, p is expressed by:

$$p = p_i + \frac{1}{3}q \tag{4.7}$$

where p_i is the mean pressure before imposing the shearing load. The relation between consolidation creep stress and shear creep stress can be derived as:

$$\sigma_{cr}^{c} = p - p_a = \frac{1}{3}\left(q - q_r\right) \tag{4.8}$$

$$\sigma_{cr}^{c} = \frac{1}{3}\sigma_{cr}^{s} \tag{4.9}$$

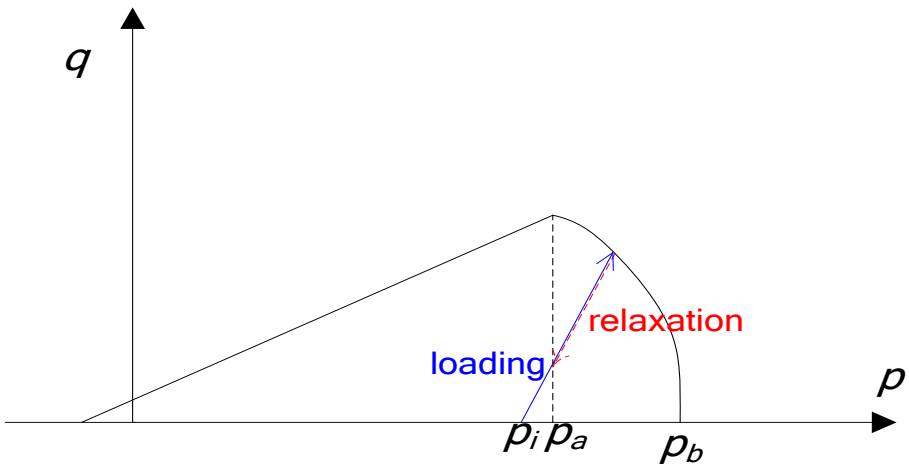

Figure 4-1 Sketch showing the stress path of a relaxation test.

During the relaxation test, the axial strain component from shear creep and consolidation creep is compensated by the component from linear elastic rebound. The consolidation creep parameters have been derived from the previous section.

$$\int_{t_a}^{t_b} A^s e^{\alpha^s \sigma_{cr}^s} \left(\frac{t_1}{t}\right)^{m^s} dt + \int_{t_a}^{t_b} A^c e^{\alpha^c \sigma_{cr}^c} \left(\frac{t_1}{t}\right)^{m^c} dt = \frac{\Delta\sigma_{11}}{E} \tag{4.10}$$

Similar to the previous procedure, the creep stress, σ_{cr}^s is a function of time, which can be derived using curve fitting based on lab data. The decreasing trend of σ_{cr}^s with the increase of time can be modeled by a simple function as:

$$\sigma_{cr}^s(t) = \frac{a}{t+b} \tag{4.11}$$

4.4. Deriving creep parameters for Regina clay soil

Hewage (2018) conducted a range of stress relaxation tests on Regina clay soil using oedometer tests and triaxial tests. Related mechanical parameters for Drucker-Prager/Cap model were also derived based his experimental measurements and included in Table 4-1. Three sets of 1D relaxation tests at different initial consolidation stresses are displayed in Figure 4-2. Before each relaxation test, a constant rate of strain (CRS) loading condition (about 3%/day) was applied to attain a vertical stress. Using the previous approach in section 4.2, the results for consolidation creep parameters are derived and included in Table 4-1.

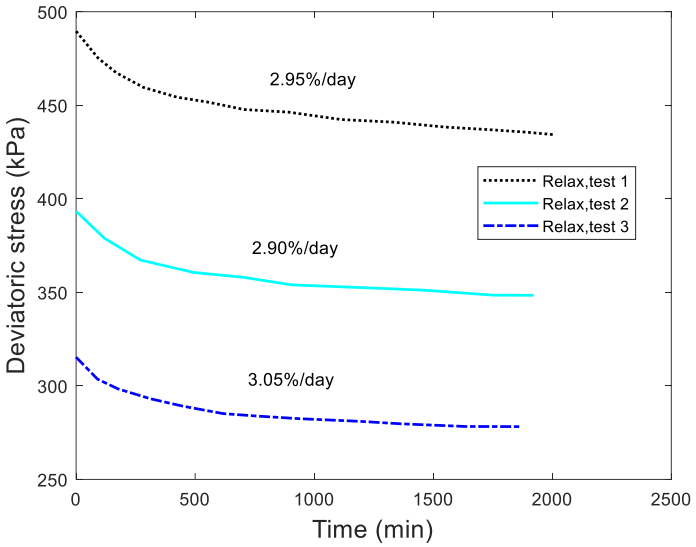

Figure 4-2 Result of stress relaxation test conducted during the oedometer test on Regina clay sample, after Hewage (2018).

The stress relaxation tests under a triaxial testing condition are displayed in Figure 4-3.

After drawing the stress path of relaxation test 1, 2 in the p-q plot, we can find that the both the shear creep and the consolidation creep are involved in the stress relaxation processes, as shown in Figure 4-4.

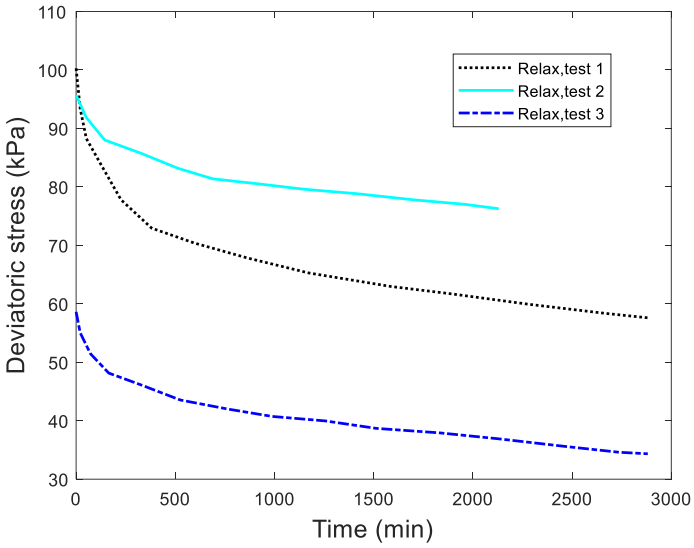

Figure 4-3 Result of stress relaxation test conducted during the shear stage of drained triaxial compression test on Regina clay sample, after Hewage (2018).

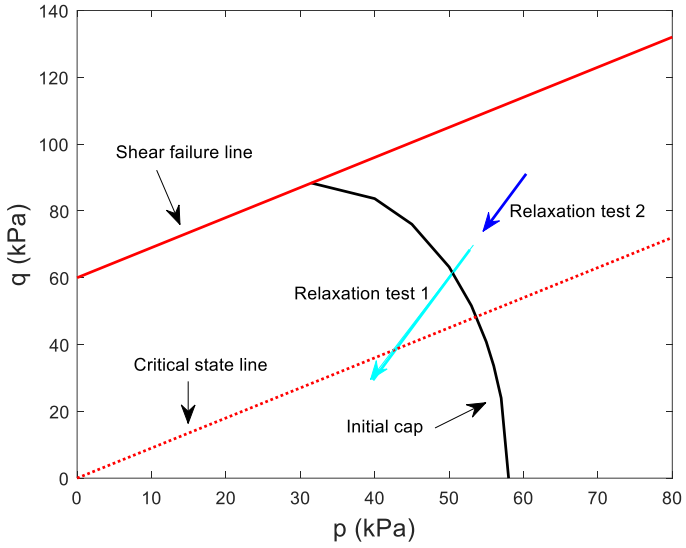

Figure 4-4 Stress path of two relaxation tests under the drained triaxial testing condition.

The shear creep parameters are obtained and listed in Table 4-1 according to the approach mentioned in the section 4.3. Those parameters will be used for the subsequent numerical modeling analysis.

Table 4-1 Material properties for constitutive modelling on Regina clay.

	Parameter	Value
Elastic	E (MPa)	15
	ν	0.3
Cap Plasticity	Cohesion, *d (kPa)*	60
	Angle of friction, β (deg)	42^o
	Cap eccentricity, R	0.3
	Transition surface radius	0
	Initial cap yield surface	0
	Flow stress ratio, *K*	1
Strain hardening	Initial void ratio, e_0	0.93
	λ	0.20
	k	0.03
	Pre-consolidation stress, p_0 (kPa)	58
consolidation creep	A^c	0.000115
	α^c(Kpa)	0.023458
	m^c	0.929771
	t_1	1
Shear creep	A^s	0.000118
	α^s(Kpa)	0.07

	m^s	0.625374
	t_l	1

5. Numerical modeling of tri-axial tests on Regina clay soil

5.1. Tri-axial tests on Regina clay soil

Hewage (2018) conducted drained tri-axial tests on Regina clay at varying strain rates. A brief introduction to the laboratory test condition is given herein. Details information including the measured procedures and results can be found in Hewage (2018).

- Preparation of instruments

For this triaxial cell, VJ tech automatic volume change measuring devices and GDS advanced pressure volume controller were used, as shown in Figure 5-1. Before starting a triaxial test series, deaerated water were filled in cell pressure supply systems and back and pressure controller in order to eliminate any remaining air inside the system.

(a)

(b)

Figure 5-1 (a) Automatic volume change devices; (b) GDS pump, from Hewage (2018).

- Preparation of sample

After compacting soil in the mould, Shelby tubes which were wrapped with plastic wrappers were driven into the compacted soil. Then, removing Shelby tubes from the mould. After that, keeping sample in a moist room until soil specimens were extruded from Shelby tubes.

- Consolidation and shearing of sample

Before shearing process, sample was isotropically consolidated to an effective confining pressure which is equal to 30kpa. During the shearing process, drainage from the top and bottom was allowed for all the samples. Axial deformation of samples can be measured by linear displacement sensor (LDS), as shown in Figure 5-2.

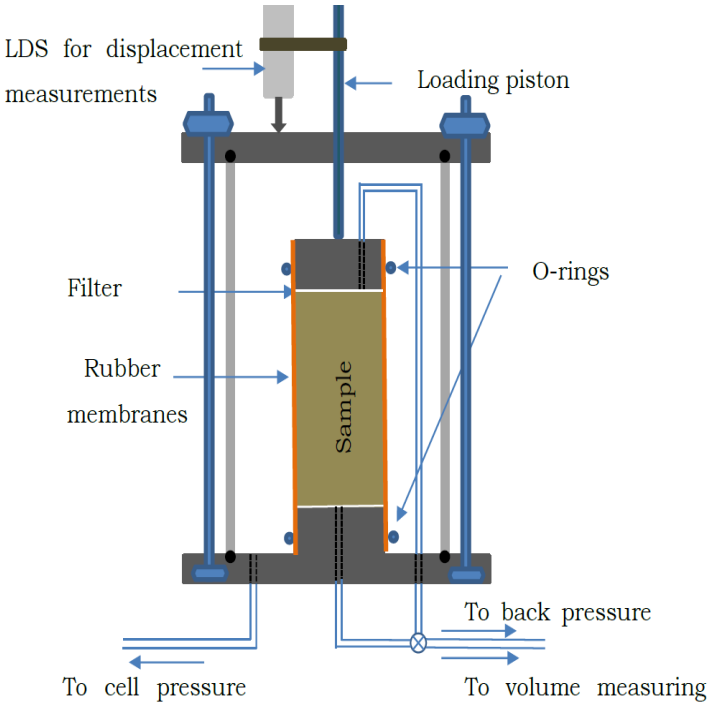

Figure 5-2 Schematic diagram of triaxial system used for drained triaxial compression tests on saturated soils, from Hewage (2018).

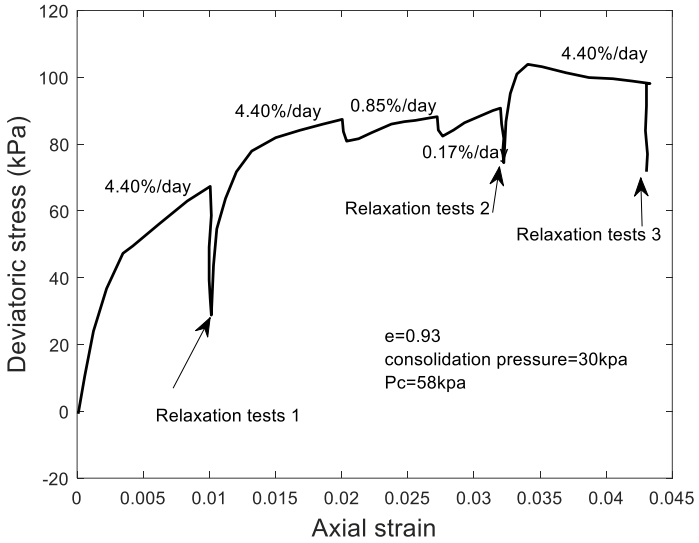

Figure 5-3 Measured strain-rate-dependent stress-strain relation of Regina clay soil, after Hewage (2018).

The measured strain-rate-dependent stress-strain relation of Regina clay soil can be found in Figure 5-3. The subsequent numerical modeling analysis were conducted to simulate this set of triaxial test using the constitutive modeling parameters described in Chapter 4.

5.2. FEM modeling

With the above-mentioned soil models and the corresponding constitutive parameters of the Regina clay soil, we were able to perform a FEM numerical model to simulate the strain-rate-dependent stress strain relations for a small sample on Regina clay under drained triaxial test condition.

The simulation was conducted using Abaqus 6.14 where the finite element method was applied. The height of a small sample is 0.09m and the diameter is 0.054m, the sizes are according to the sample size from Hewage (2018).In ABAQUS simulation, the three-dimensional asymmetric mesh is used with this small sample. The element chosen is a 3D stress 8-node linear brick element with hourglass control, and reduced integration, as shown in Figure 5-4.

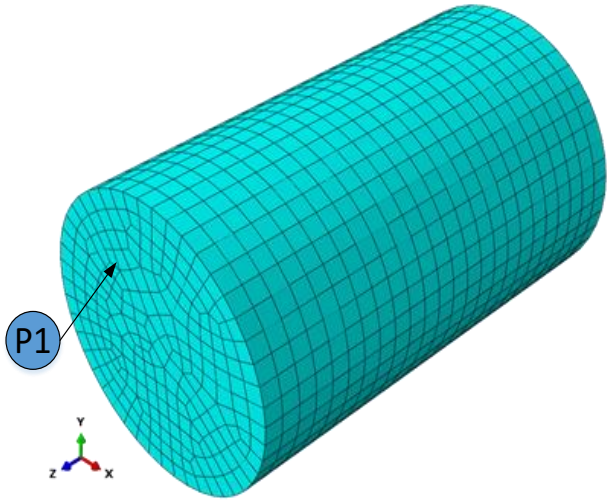

Figure 5-4 Sketch showing the configuration, mesh, and one monitoring points of the studied problem.

The boundary conditions of the finite element shown in Figure 5-5 are as follows. On the bottom side, the vertical and horizontal component of the displacement is fixed ($u_x = u_y = 0$).

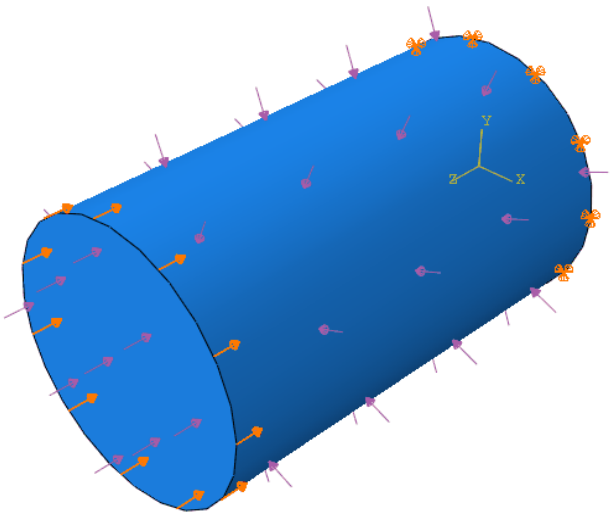

Figure 5-5 Boundary conditions of the finite element.

Similar to an actual consolidated – drained triaxial test, this finite element analysis is carried out in two steps: a consolidation step and a shearing step. Pore water pressure was not considered in this study since we are focusing on the mechanical behavior under the drained stress path condition. In the first step, the confining pressure of 30 kPa was applied at the top surface and the surrounding surface of the mesh. Step 2 is the shearing step with duration of 0.96, 4.83, 24.138days as examples. On the top surface a uniform downward displacement of 0.0039 m was applied. In this step the loading plate is forced to displace downward at a different strain rates.

The ABAQUS results are shown below for the different boundary conditions. Figure 5-6 shows a comparison of the modeled Mises stress distributions in Regina clay soil subjected to strain rates. It is evident a slightly lower value of Mises stress can be found for the case with a lower strain rate (24.138 days).

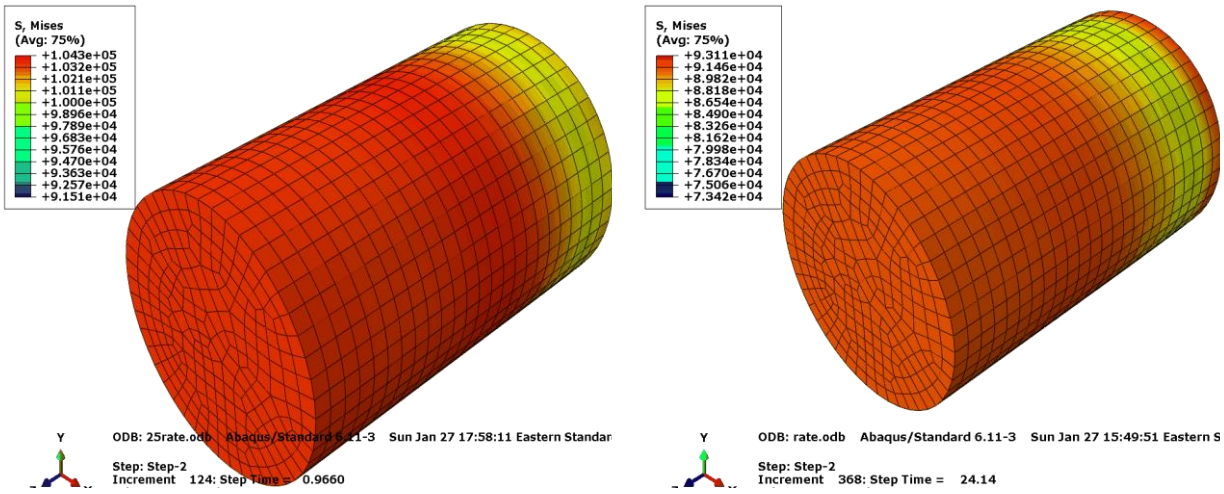

(a) (b)

Figure 5-6 Modeled Mises stress (in Pa) distributions in Regina clay soil using (a) 0.966 day and (b) 24.138 days.

The similar situation can also be found for plastic shear strain, as shown in Figure 5-7. The bigger value of plastic shear strain can be found for the case with a lower strain rate (24.138 days).

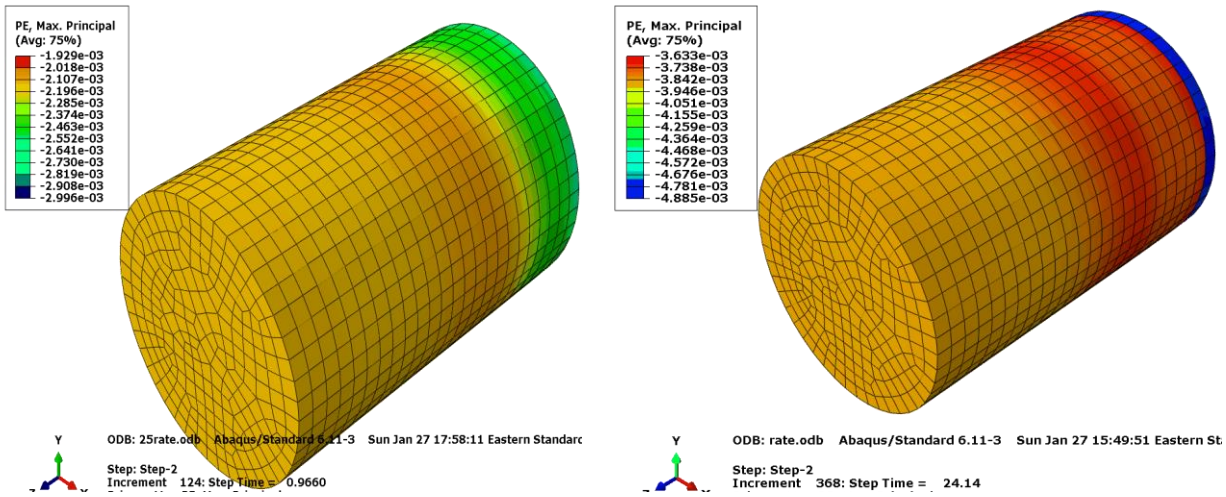

(a) (b)

Figure 5-7 Modeled plastic strain distributions in Regina clay soil using (a) 0.966 day and (b) 24.138 days.

At a given vertical displacement, the different strain rates would cause different creep strains, as shown in Figure 5-8. The shear stress for the case with more creep behavior (24.138 days) is always lower than the case with less creep (0.966 day).

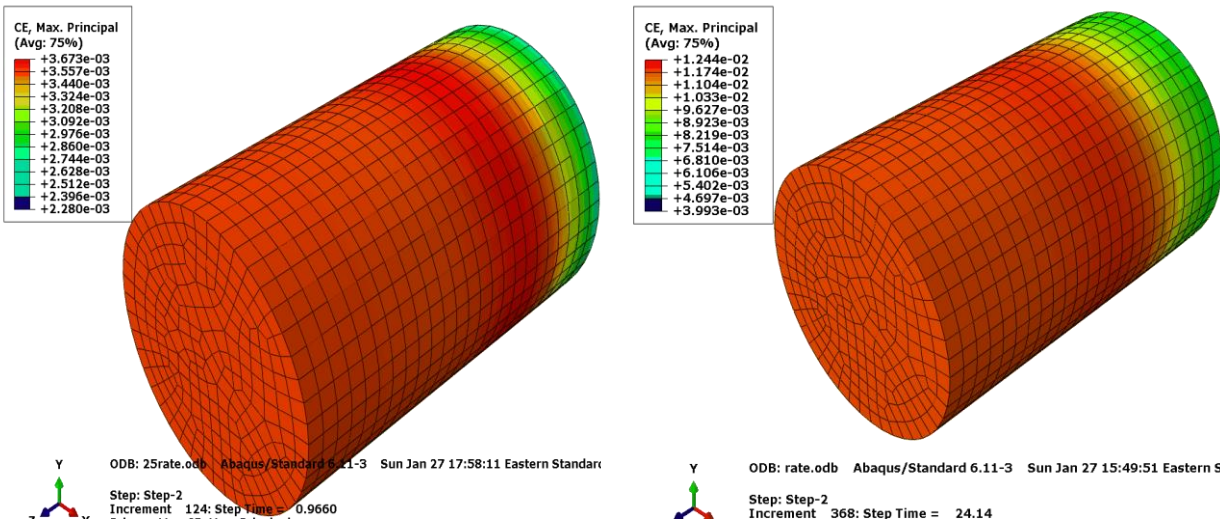

(a) (b)

Figure 5-8 Modeled creep strains in Regina clay soil using (a) 0.966 day and (b) 24.138 days.

The stress path for monitoring point1 is shown in Figure 5-9. The curve shows that the stress path for point 1 increase gradually to touch the shear failure line.

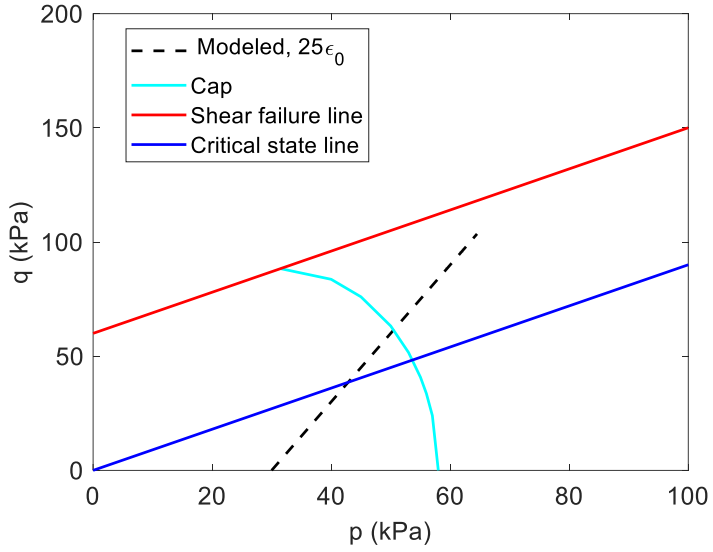

Figure 5-9 Modeled stress paths of monitoring point 1 in p–q space.

The calculated consolidated – drained stress – strain behavior of the clay specimen is shown in below Figures 5-10, 5-11 which compared with the measured data according to the experimental results of Hewage (2018). The axial strain versus volumetric strain is also shown in the Figure 5-11. This means that the Drucker-Prager model combining with the Singh-Mitchell creep model embodied in the finite element method is capable of describing the consolidated – drained triaxial behavior of soft clays. However, the volumetric-axial strain relations cannot be well simulated using Drucker-Prager/Cap model combined with Singh-Mitchell creep model.

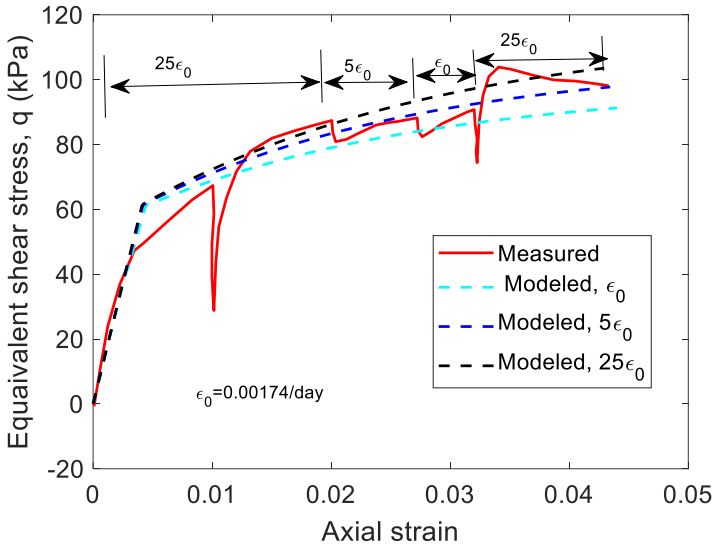

Figure 5-10 Modeled and measured stress-strain relations for a Regina clay sample.

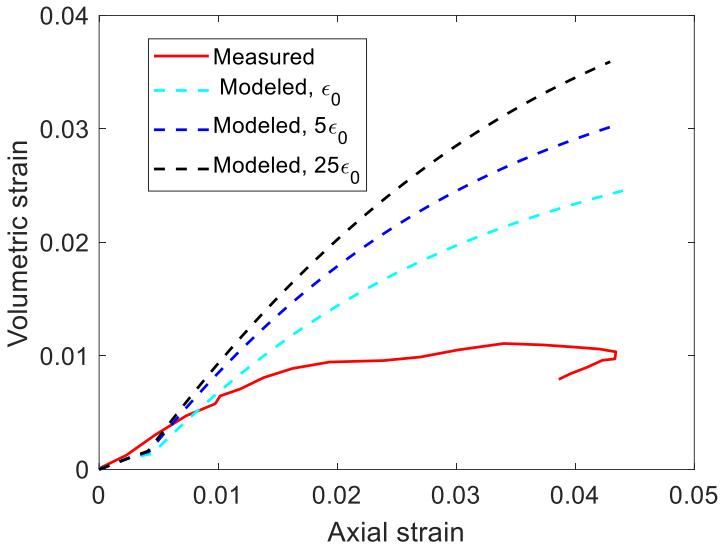

Figure 5-11 Modeled volumetric-axial strain relations for numerical tests under different strain rates.

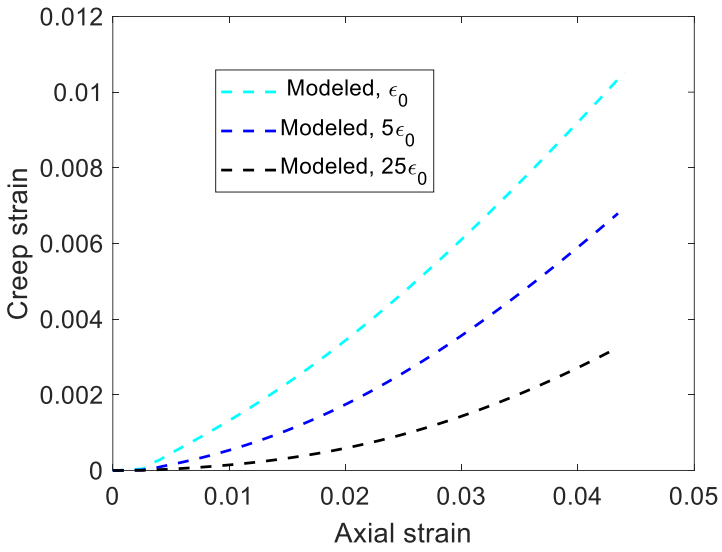

Figure 5-12 Modelled total-creep axial strain relations for numerical tests under different strain rates.

It is clear that the sample displays a higher strength at a higher strain rate (Figure 5-10). The difference is due to the creep behavior, where the sample will have more creep strain for lower

strain rate test condition (Figure 5-12). However, the creep strain components cannot be exported from Abaqus. It's not clear whether the strain is from shear creep or consolidation creep.

Abaqus 6.14 not only can simulate the simple consolidated – drained triaxial test, but also can analysis the consolidated – drained triaxial test includes relaxation behavior. This finite element analysis is carried on the same Regina clay which carries out in several steps: as shown in Table 5-1.

Table 5-1 Step information of relaxation tests in Abaqus.

Name	Procedure	Time
Consolidation step	Static, General	1
Shearing step 1	Visco	0.25
Relaxation step 1	Visco	6
Shearing step 2	Visco	0.23
Shearing step 3	Visco	0.8
Shearing step 4	Visco	2.3
Relaxation 2	Visco	2.8
Shearing step 5	Visco	0.25425

Same as the simple triaxial drained consolidation test, in the first step, the confining pressure of 30 kPa was applied at the top surface and the surrounding surface of the mesh. Pore water pressure was not considered in this study since we are focusing on the mechanical behavior under the drained stress path condition.

For the shearing step1, a uniform downward displacement of 0.001m was applied on the top surface, and to keep the displacement in relaxation step1. In the next step, adding a

displacement of 0.0189m on the top surface of sample, which was to keep strain rate at $25\varepsilon_0$ followed by a strain rate of $5\varepsilon_0$ for the next step. In the shearing step 4, the strain rate was equal to ε_0. After putting different strain rate in the shear steps, one more relaxation step was added. Finally, a strain rate of $25\varepsilon_0$ was re-applied.

Compared with the measured data according to the experimental results of Hewage (2018), the calculated consolidated – drained stress – strain behavior of the clay specimen is shown in below Figure 5-13.

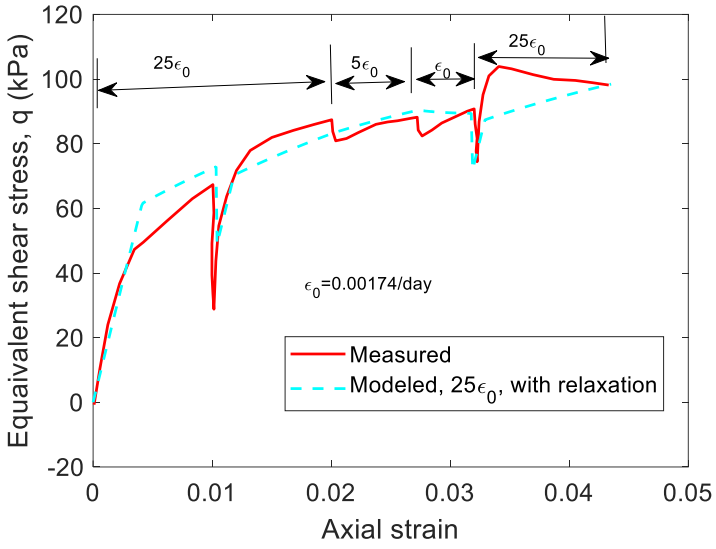

Figure 5-13 Relationship between equivalent stress and axial strain by different strain rates.

This means that the Drucker-Prager model combining with the Singh-Mitchell creep model embodied in the finite element method is capable of describing the consolidated – drained triaxial behavior considering stress relaxation behaviors on soft clays.

5.3. Summary

Under a drained stress path condition, strong strain-rate-dependent behavior is significant in soft clay soil like the Regina clay. The Drucker-Prager/Cap model combined with Singh-Mitchell creep model can be used to simulate the strain-rate-dependent stress-strain relations for soft clays by considering both shear and consolidation creep mechanisms. The volumetric-axial strain relations cannot be well simulated using Drucker-Prager/Cap model combined with Singh-Mitchell creep model. Stress relaxation tests can be applied to effectively and efficiently estimate creep parameters using facilities for the oedometer test and the triaxial test.

6. Bearing capacity analysis of a strip foundation

As the population increases, people tend to build on soft clay deposits which was previously treated unsuitable for residential housing and construction projects (Fang 2013). The mechanical behavior of soft clays is highly dependent on the applied stress path and strain rate, which make soft clay soils display strong viscoplastic behavior (Fodil et al. 1998, Yin and Graham 1999, Yin et al. 2011). An accurate characterization of the complex shear and consolidation behavior of clay soil is critical for a foundation's bearing capacity analysis (Taiebat and Carter 2000). Most previous studies focus on elastic-viscoplastic behavior of clay soil under an undrained stress path condition (Yin and Graham 1999, Yin et al. 2010, Yin et al. 2011). The developed constitutive models cannot simulate the strong time dependent stress-strain relation of soft clay under drained stress path condition. In the long-term bearing capacity analysis for a shallow foundation, the neglect of the time dependent stress-strain relation of soft clay may result in inaccurate result. In this study, we performed finite element modeling on the bearing capacity of a shallow foundation on soft clay using Drucker-Prager/Cap model combined with Singh-Mitchell creep model.

6.1. Analytical solution based on Terzaghi's bearing capacity equation

Terzaghi (1951) presented his bearing capacity equation for shallow foundations, as shown in Figure 6-1, which was derived for a continuous (strip) foundation with general shear failure.

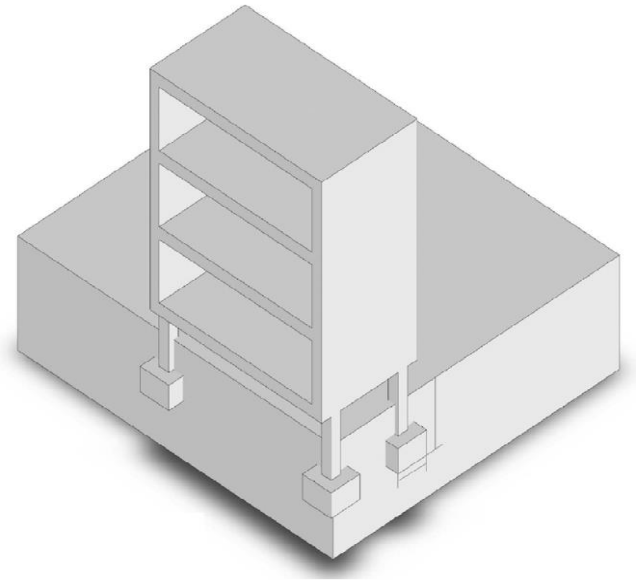

Figure 6-1 Sketch showing a typical shallow foundation, from Helwany (2007).

The Figure 6-2 shows the assumed failure surface which underlying the foundation. Three distinct failure zones of soil under the footing: a triangular zone, DEH, which is immediately under the footing; two radial zones, DHG and EIH; and two Rankine passive zones, DGC and EFI.

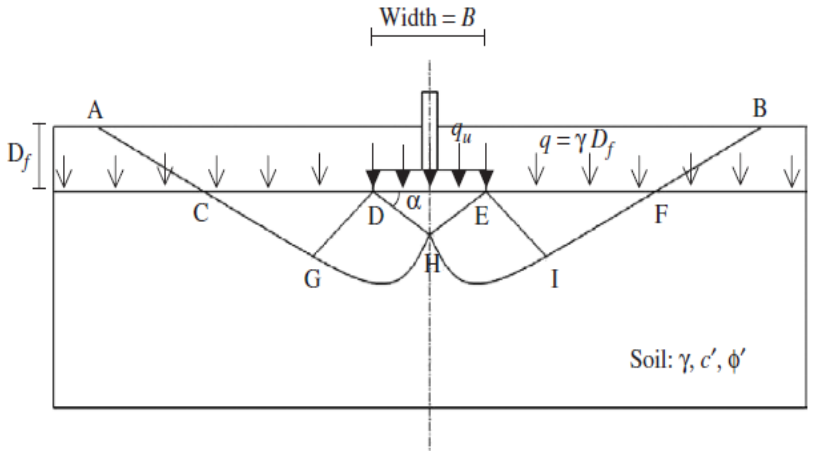

Figure 6-2 General shear failure of a strip foundation: Terzaghi's assumptions, from Terzaghi (1951).

In his assumption, the angle α is assumed to be equal to the soil angle of internal friction φ, the soil shear resistance along CA and FB is neglected. Terzaghi (1951) assumed that the bearing capacity of the foundation is the pressure of the foundation which will cause the triangular zone to be in a downward impending motion condition. When that happens, then the triangular zone will push the radial shear zones to the left and right away from the footing, and therefore, the radial shear zones will push the Rankine passive zones upward. The impending motion condition is assumed to take place in all zones at the same time. Based on this limited assumption, Terzaghi derived the following equation for a strip foundation and general shear failure:

$$q_u = c' N_c + qN_q + \frac{1}{2}\gamma B N_\gamma \tag{6.1}$$

Where c' is the cohesion intercept of soil, q is the overburden pressure at foundation depth, γ is the unit weight of soil, B is the foundation width, and N_c, N_q, and N_γ are non-dimensional bearing capacity factors that are functions of soil friction angle φ.

$$q = \gamma D_f \tag{6.2}$$

$$N_q = e^{\pi \tan\phi} \tan^2(45 + \frac{\phi}{2}) \tag{6.3}$$

$$N_c = (\mathrm{N}_q - 1)\cot\phi \tag{6.4}$$

$$N_\gamma = (\mathrm{N}_q - 1)\tan 1.4\phi \tag{6.5}$$

The bearing capacity for a strip foundation is given as:

$$q_u = c' N_c + qN_q + 0.5\gamma B N_\gamma \tag{6.6}$$

So for the 20m*10m strip foundation, from the equation 3-20, we can get ϕ =23, c =9kpa. Therefore, by using these equations, we can get q=58kpa, N_q=8.655kpa, N_c=18kpa, N_r=4.8kpa, q_u=724kpa

6.2. FEM modeling

With the soil models and the corresponding constitutive parameters of Regina clay soil included in previous chapters, we were able to perform a numerical analysis of a limit equilibrium solution for layers of Regina clay which was loaded by a rigid, perfectly rough footing. The simulation was conducted using Abaqus 6.14 where the finite element method was applied, and the problem was treated in 2D plane strain condition. The model assumes symmetry about a center plane. Shown in Figure 6-3, the modeled Regina clay soil formation is 10 m in deep and 10 m in width. The shallow foundation is a 1-m-thick rigid and perfectly rough plate that spans a 1m on the top-left side of soil layers. The strip foundation is assumed to be in perfect contact with the soil, which means that relative displacement between the foundation and soil is not permitted. Reduced-integration bilinear plane strain quadrilateral elements are used for the soil. The mesh is set finer in the vicinity of the foundation because as this zone bears most of the stress concentration (Figure 6-3). Four monitoring points (P1， P2, P3 and Point4) were selected for tracking the stress paths. An inspect of mesh convergency has been conducted for the simulation.

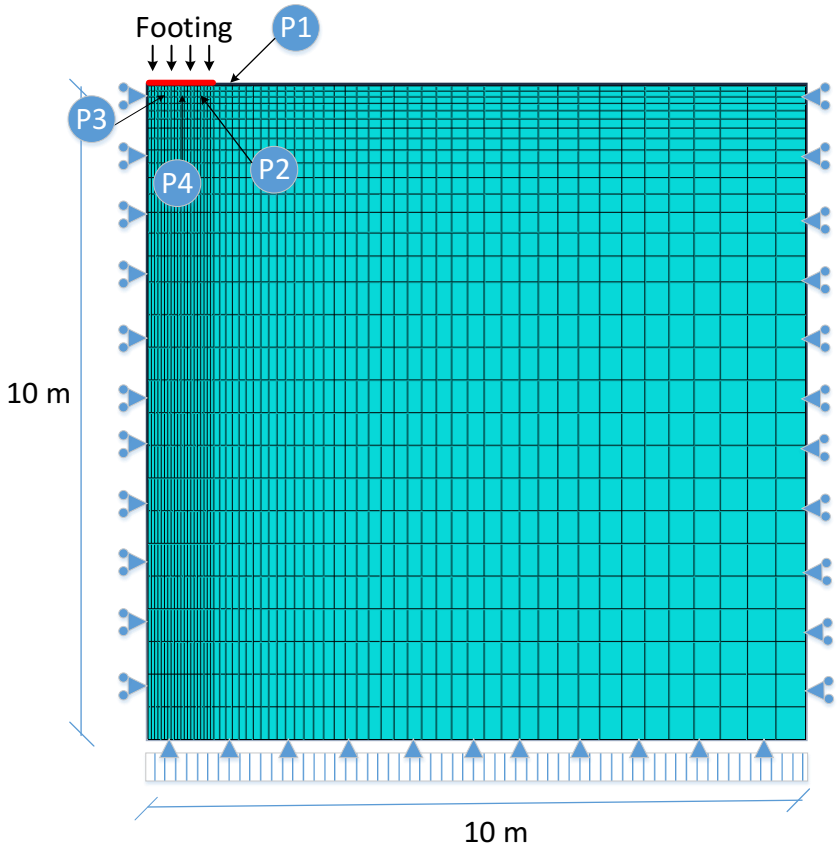

Figure 6-3 Sketch showing the configuration, mesh, and two monitoring points of the studied problem.

This ABAQUS model divide to 15 parts from the top to the bottom, which corresponds to the different hydrostatic compression yield stress. The hydrostatic compression yield stress (pre-consolidation stress) in the top 3 m is the same (58 kPa), and this pre-consolidation stress increases with an increase of buried depth below 3 m. The relationship between hydrostatic compression yield stress and the height is shown in Figure 6-4.

$$Pb_{i+1} = Pb_i + rh \tag{6.7}$$

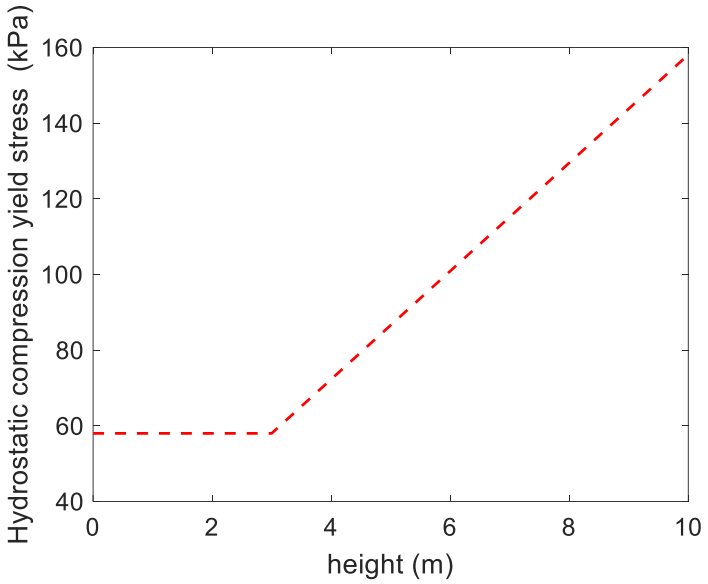

Figure 6-4 Relationship between the height and mean effective stress.

For the boundary conditions, the base of the soil layer is fixed in both the horizontal and vertical directions. The right and left vertical boundaries are fixed in the horizontal direction but free in the vertical direction. In the beginning of the analysis, a surcharge load with a pressure of 57 kPa was applied to the top surface of soil layer and a gravity load was applied to the whole soil body. Pore water pressure was not considered in this study since we are focusing on the mechanical behavior under the drained stress path condition.

After the completion of surcharge and gravity loads, a displacement of 0.85 m was applied on the 1m wide foundation part using different time intervals (1 day, 30 days, and 60days). Until some soil element in the vicinity of the corner of the foundation have severely distorted, the foundation pressure can be increased gradually up to the failure point (termed the *bearing capacity*) at which a failure surface. In the present finite element analysis, such a failure surface is evident when the plastic shear strains are plotted for the at-failure condition as shown in Figure 6-5.

Smaller values of plastic shear strain can be found for the case with a lower strain rate (30days, 60 days).

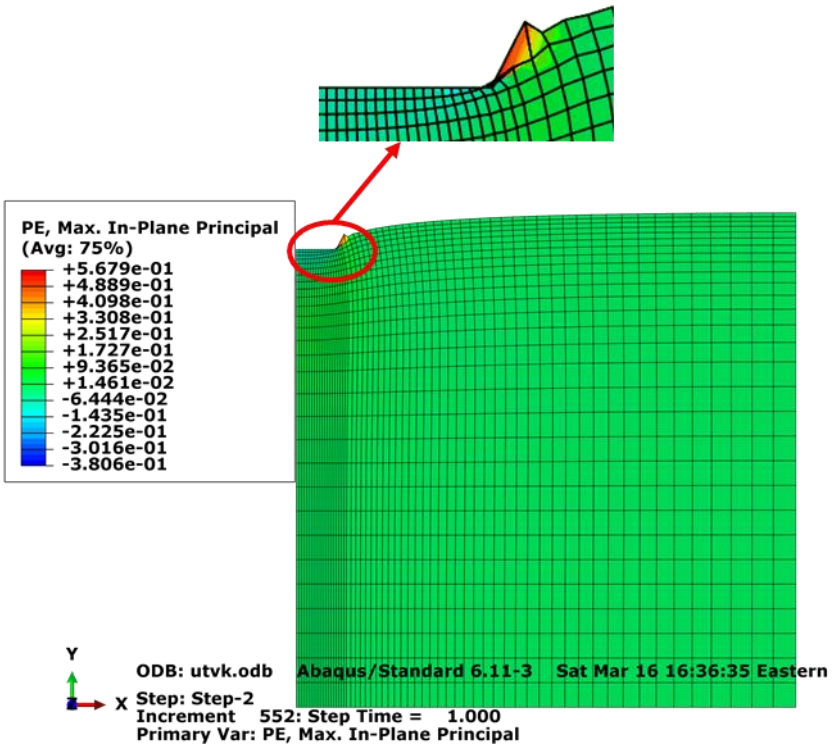

(a)

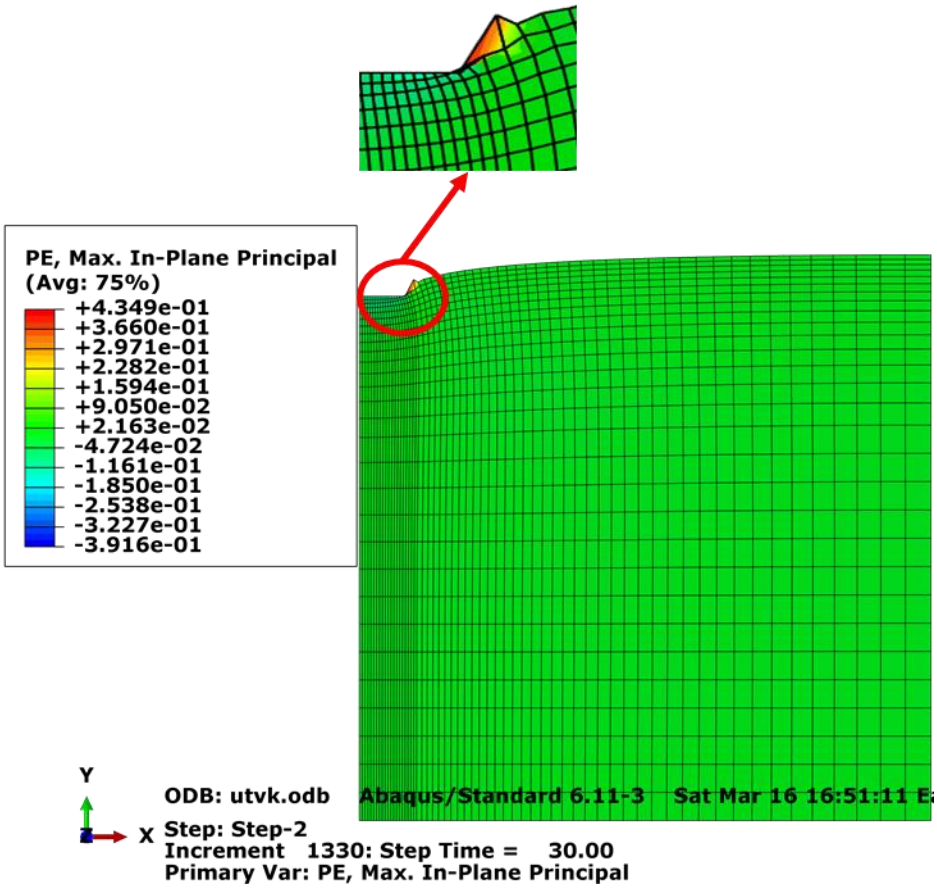
PE, Max. In-Plane Principal
(Avg: 75%)
+4.349e-01
+3.660e-01
+2.971e-01
+2.282e-01
+1.594e-01
+9.050e-02
+2.163e-02
-4.724e-02
-1.161e-01
-1.850e-01
-2.538e-01
-3.227e-01
-3.916e-01
Y
X
ODB: utvk.odb
Abaqus/Standard 6.11-3
Sat Mar 16 16:51:11 E
Step: Step-2
Increment 1330: Step Time = 30.00
Primary Var: PE, Max. In-Plane Principal

(b)

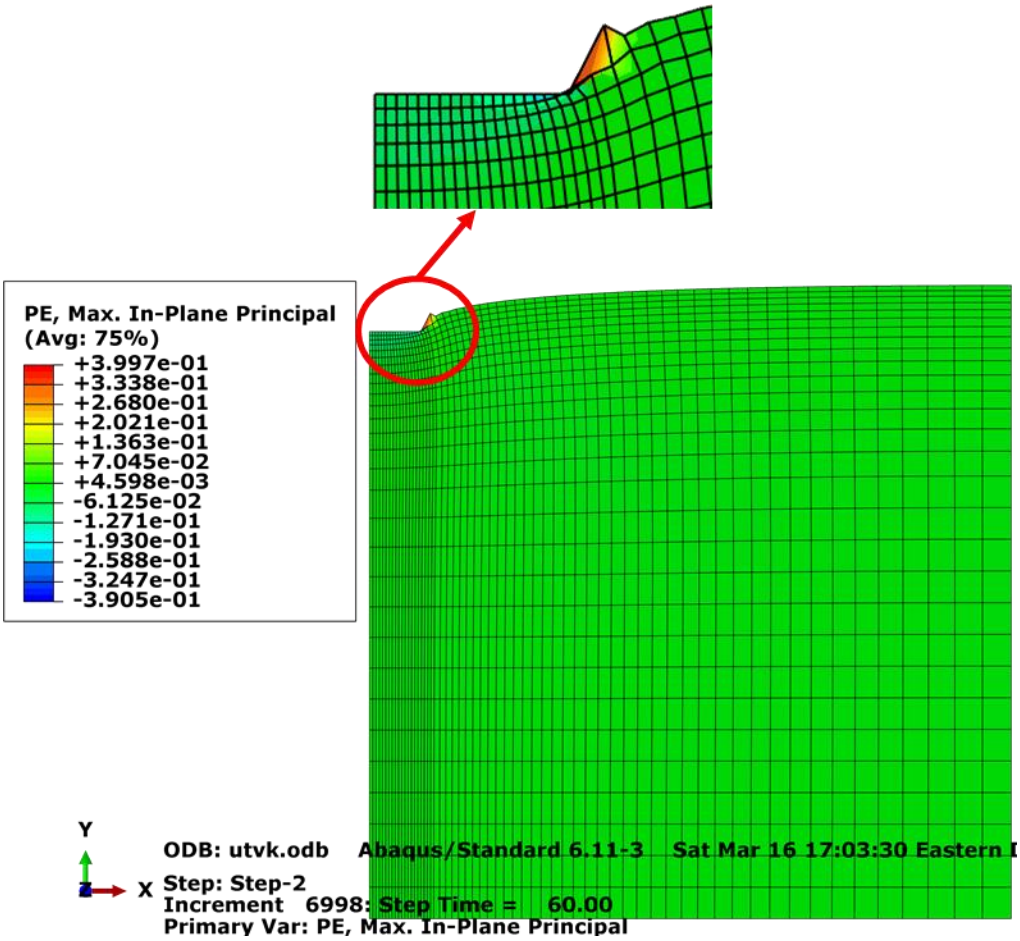

(c)

Figure 6-5 Modeled plastic shear strain distributions in Regina clay soil using (a) one day (b) 30 days (c) 60 days.

The different boundary condition applied to the top surface of foundation causes different bearing capacity-displacement results (Figure 6-6).

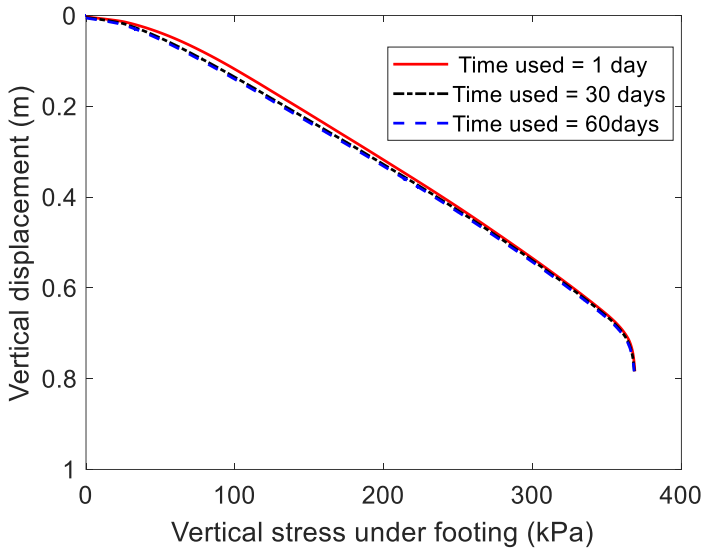

Figure 6-6 Modeled load-displacement curve for the studied footing problem using different time intervals.

The results display that there is no difference in the ultimate bearing capacity (368 kPa) for those cases using different strain rates. However, the vertical stress for the case with more creep behavior (30 days and 60 days) is always lower than the case with less creep (1 day). At a given vertical displacement, for instance 0.2 m, the developed vertical stress for the one with a lower strain rate (60 days) gets 10 kPa less than the one with a higher strain rate (1 day). A comparison of the modeled Mises stress distributions in Regina clay soil subjected to strain rates are displayed in Figure 6-7. A slightly lower value of Mises stress can be found for the case with a lower strain rate (30days, 60 days).

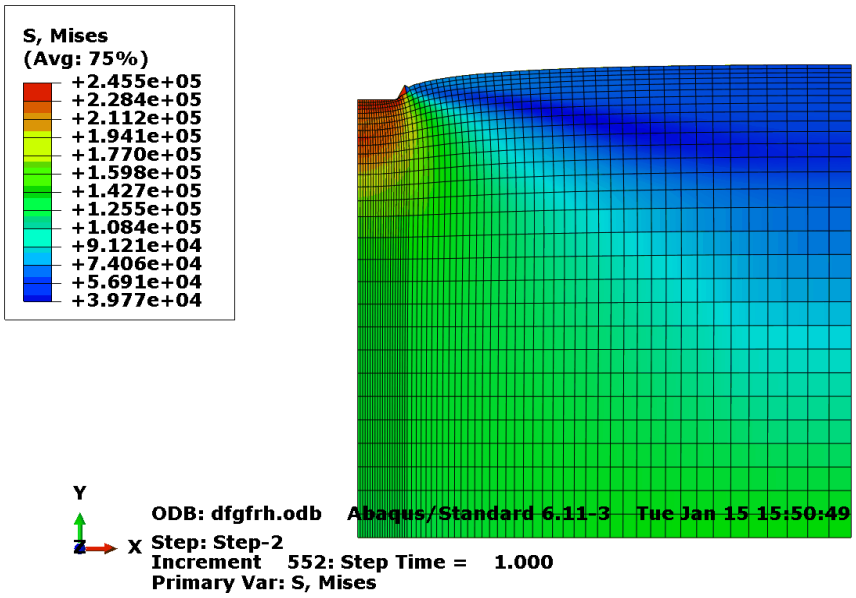
S, Mises
(Avg: 75%)
+2.455e+05
+2.284e+05
+2.112e+05
+1.941e+05
+1.770e+05
+1.598e+05
+1.427e+05
+1.255e+05
+1.084e+05
+9.121e+04
+7.406e+04
+5.691e+04
+3.977e+04
Y
Z
X
ODB: dfgfrh.odb Abaqus/Standard 6.11-3 Tue Jan 15 15:50:49
Step: Step-2
Increment 552: Step Time = 1.000
Primary Var: S, Mises

(a)

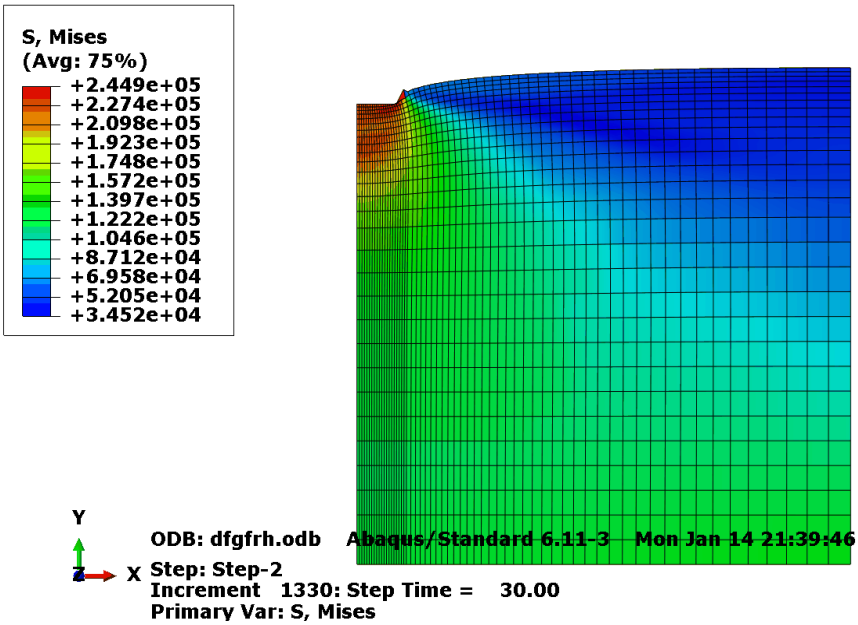
S, Mises
(Avg: 75%)
+2.449e+05
+2.274e+05
+2.098e+05
+1.923e+05
+1.748e+05
+1.572e+05
+1.397e+05
+1.222e+05
+1.046e+05
+8.712e+04
+6.958e+04
+5.205e+04
+3.452e+04
Y
Z
X
ODB: dfgfrh.odb Abaqus/Standard 6.11-3 Mon Jan 14 21:39:46
Step: Step-2
Increment 1330: Step Time = 30.00
Primary Var: S, Mises

(b)

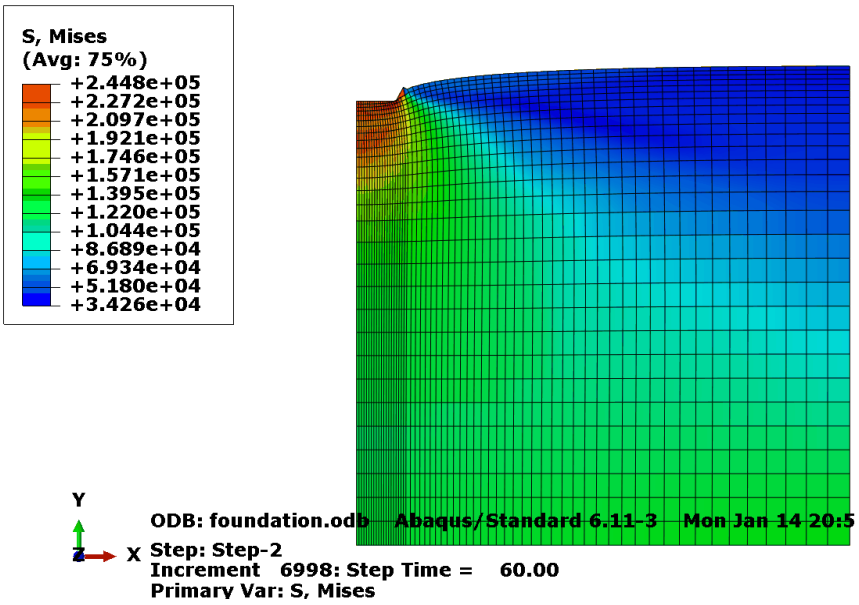

(c)

Figure 6-7 Modeled Mises stress (in Pa) distributions in Regina clay soil using (a) one day (b) 30 days (c) 60 days.

Similar situation was noticed for the volumetric inelastic strain in Regina clay (Figure 6-8), where the one with a lower strain rate (60 days) displayed less volumetric plastic strain.

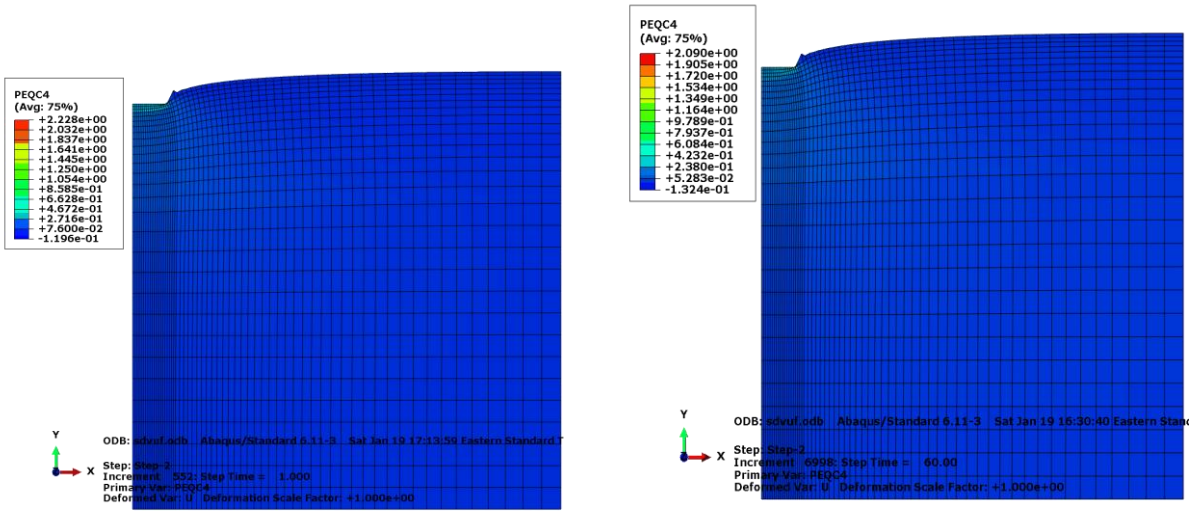

(a) (b)

Figure 6-8 Modeled total volumetric inelastic strain in Regina clay soil using (a) one day (b) 60days (PEQC4 stands for volumetric inelastic strain in Abaqus).

Similarly, Figure 6-9 shows the creep strain in vertical direction in Regina clay, where the one with a lower strain rate (60 days) displayed more creep strain.

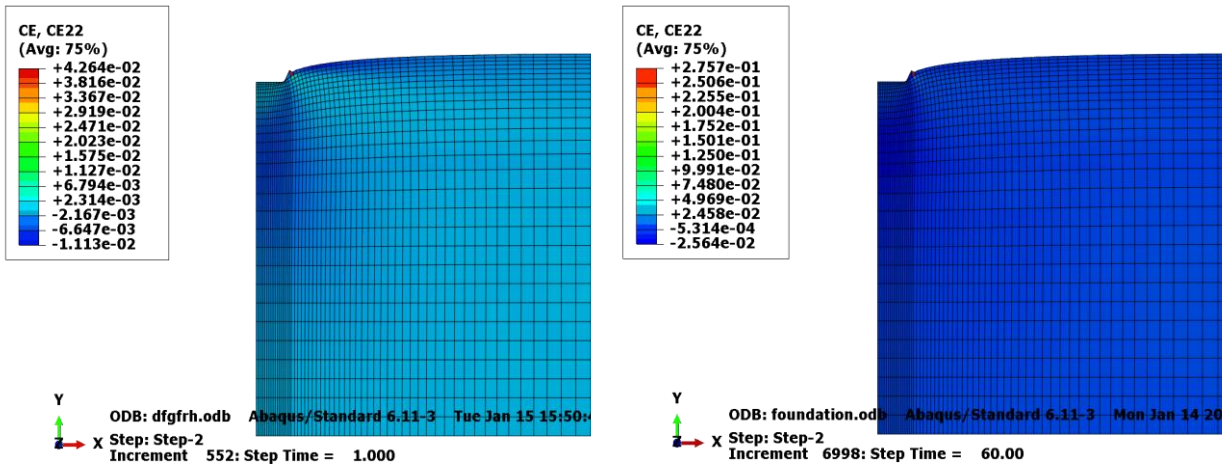

(a) (b)

Figure 6-9 Modeled creep strain in Regina clay soil using (a) one day (b) 60days (CE2 stands for creep strain in vertical direction in Abaqus).

When we compare the reaction force distribution in Regina clay, we can find the one with a lower strain rate (60 days) displayed bigger reaction force, as shown in Figure 6-10.

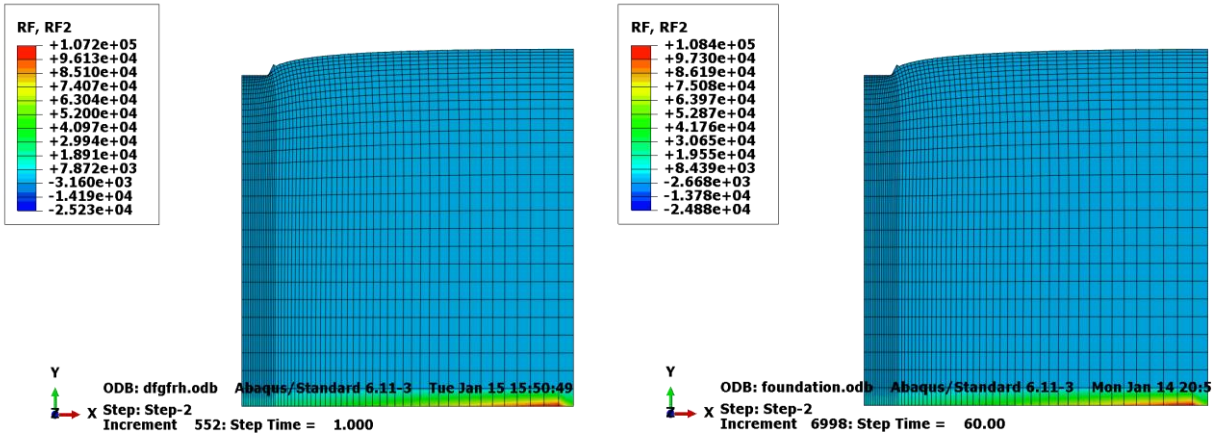

(a) (b)

Figure 6-10 Modeled reaction force in Regina clay soil using (a) one day (b) 60days (RF2 stands for reaction force in vertical direction in Abaqus).

According to the Figure 6-11, the one with a lower strain rate (60 days) displayed smaller equivalent plastic strains for Drucker-Prager failure surface in Regina clay soil.

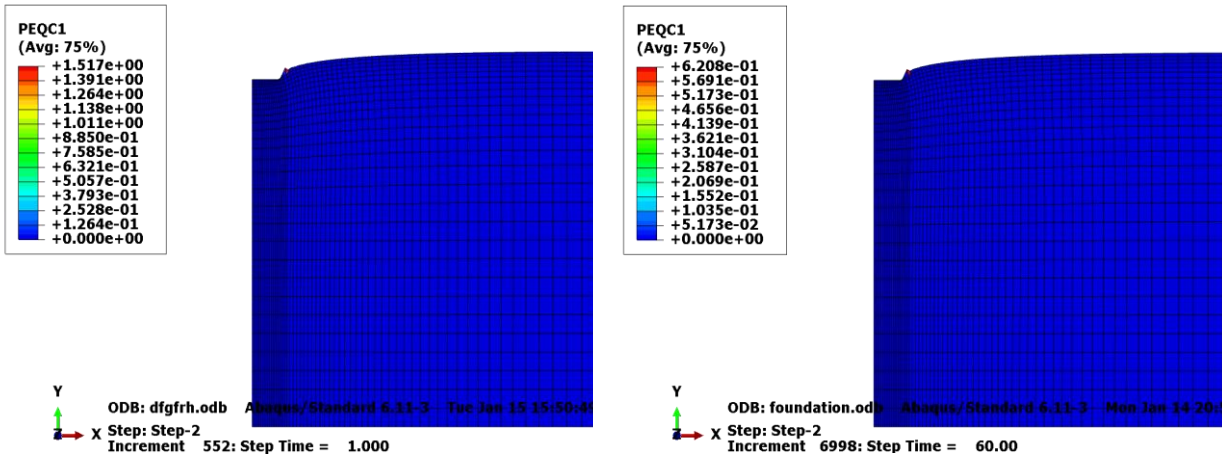

(a) (b)

Figure 6-11 Modeled equivalent plastic strains for Drucker-Prager failure surface in Regina clay soil using (a) one day (b) 60days (PEQC1 stands for equivalent plastic strains for Drucker-Prager failure surface in Abaqus).

A plot of the stress paths of four monitoring points can be found in Figure 6-12. The curve shows that the generated creep behavior (for the cases with longer time intervals) affects the built of shear stress. However, they attain the same ultimate shear stress when soil gets failure.

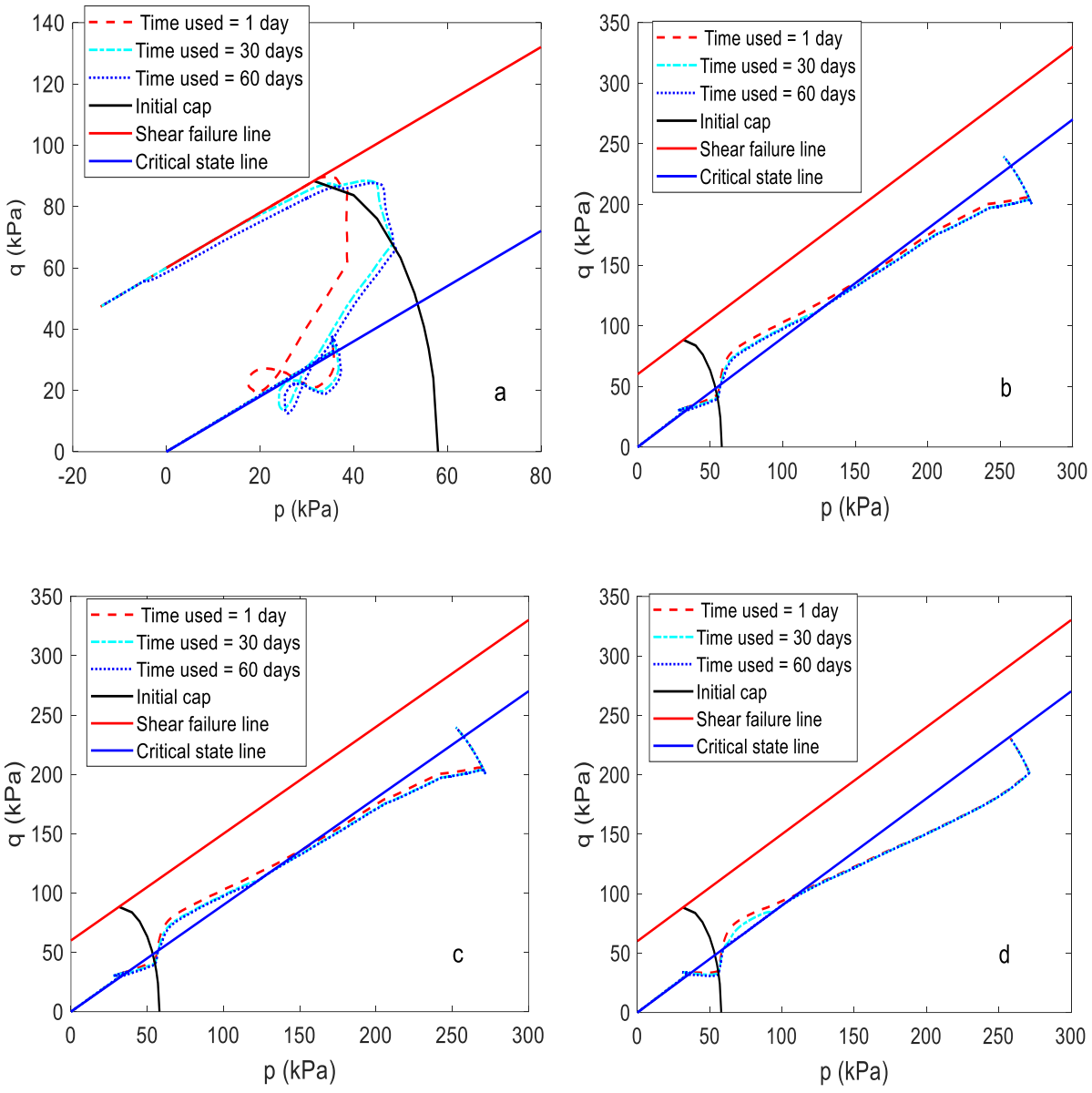

Figure 6-12 Modeled stress paths of (a) monitoring point 1 (b) monitoring point 2 (c) monitoring point 3 in p–q space (d) monitoring point 4 in p–q space in p–q space.

6.3. Comparison and summary

For the ABAQUS results, the bearing capacity is around 368kpa when step 2 is equal to 1 day, 10 days, 30 days and 60 days, in terms of the displacement is equal to 0.85m. The result is shown in Figure 6-13.

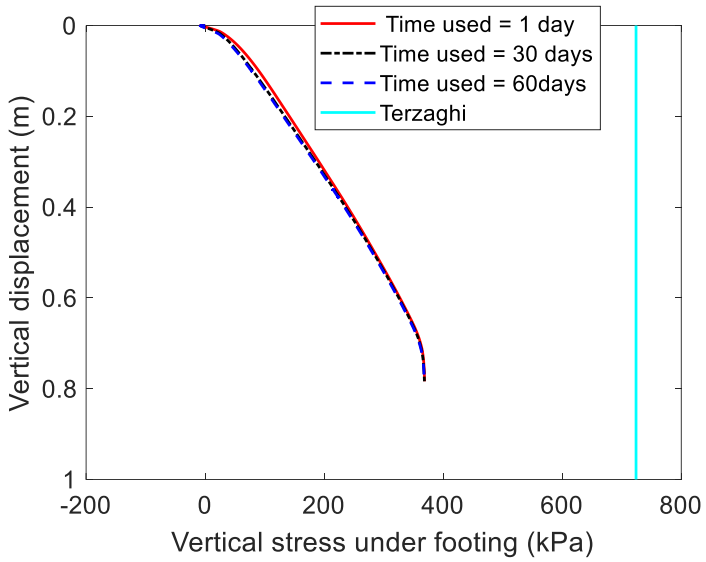

Figure 6-13 FEM results and the Terzaghi's results for the bearing capacity.

It is noticed that the finite element prediction of bearing capacity is significantly smaller than Terzaghi's bearing capacity. There are several reasons which can cause this result, the most important of the reason is that Terzaghi's equation assumes that the soil is a rigid – perfectly plastic material which fails abruptly when the bearing capacity of the soil is reached. However, the present finite element analysis assumes that the soil is an elastic viscoplastic material with hardening. Therefore, this material will deform under applied loads, which is opposed to a rigid material that does not deform. What's more, the soil can yield in a progressive manner because of the nature of the finite element formulation—elements can yield gradually and progressively.

7. Conclusions and recommendations for future work

7.1. Conclusion

The time-dependent stress-strain behavior of clay soils under the drained stress path condition is an important part of geotechnical engineering. Modified Drucker-Prager/Cap model can simulate the stress path under drained conditions with considering of creep soil behavior. Singh-Mitchell creep model could both analyze the consolidation creep and cohesion creep mechanics. A simplified approach has been proposed to derive creep parameters from stress relaxation tests. Constitutive modelling on Regina clay soil at different scales has been investigated in this study using Abaqus. Several conclusions are drawn as the following:

Deriving creep parameters from relaxation tests

Creep parameters can be effectively and efficiently estimate from stress relaxation tests using facilities. The first three parameters (A^s, α^s, m^s) can be derive from oedometer relaxation tests. The last three parameters (A^c, α^c, m^c) can be estimated from triaxial tests, where both consolidation plastic strain and shear plastic strain will be generated. The derivative free method can be applied to figure out creep parameters from stress relaxation tests data.

Constitutive modeling on elasto-viscoplastic behavior of Regina clay

The Drucker-Prager/Cap model combined with Singh-Mitchell creep model can be used to simulate the strain-stress relations on soft clay with considerations of consolidation creep and shearing creep behaviors. It is clear that the sample displays a higher strength at a higher strain rate. The difference is due to the creep behavior, where the sample will have more creep strain for lower strain rate test condition. However, the volumetric strain-axial strain relations cannot be well simulated with Drucker-Prager/Cap model combined with Singh-Mitchell creep model.

Bearing capacity analysis of a strip foundation

A numerical analysis of the bearing capacity of a shallow foundation on Regina clay soil shows that the considering of viscoplastic behavior of clay soils does not affect the ultimate bearing capacity. However, the vertical stress for the case with more creep behavior is always lower than the case with less creep. Considering from a conservative engineering point of view, viscoplastic behavior of clay soils can yield the lower bound of developed shear stress of a shallow foundation.

7.2. Recommendations for Future Work

Because of the strain-rate dependent and large time-dependent deformations of soft clay, the elastic viscoplastic behavior of soft clay soil should be studied further in details for the benefit of the construction on soft clay. The following recommendations are made for future work:

In this study, it's not clear whether the strain is from shear creep or consolidation creep because the creep strain components cannot be exported from ABAQUS. Therefore, more research is required to analysis the creep components.

Similarly, Drucker-Prager/Cap model combined with Singh-Mitchell creep model cannot well simulated the volumetric strain-axial strain relations. Further research is also required to investigative this phenomenon.

In the current study, the bearing capacity analysis of a shallow foundation on Regina clay soil shows that the considering of viscoplastic behavior of clay soils does not affect the ultimate bearing capacity. However, it is recommended to apply such viscoplastic model to simulate other geotechnical problems where shear plastic strain plays a major role for the factor of safety (e.g., slope stability analysis).

References

Abaqus. (2016). Abaqus theory manual, Simulia.

Adachi, T., and Okano, M. (1974). A constitutive equation for normally consolidated clay. *Soils and Foundations*, **14**(4): 55-73.

Al-Darzi, S.Y.K., Bangash, M., Desayi, P., Krishnan, S., Hognestad, E., Kohnke, P., Liu, Y., Willam, K., Warnke, E., and Zienkiewicz, O. (1989). Associated and non-associated visco-plasticity and plasticity in soil mechanics. *Journal of Applied Sciences*, **7**(5): 345-350.

Augustesen, A., Liingaard, M., and Lade, P.V. (2004). Evaluation of time-dependent behavior of soils. *International Journal of Geomechanics*, **4**(3): 137-156.

Azari, B., Fatahi, B., and Khabbaz, H. (2014). Assessment of the elastic-viscoplastic behavior of soft soils improved with vertical drains capturing reduced shear strength of a disturbed zone. *International Journal of Geomechanics*, **16**(1): B4014001.

Bjerre, J. (2015). Development and Evaluation of an Effective Stress Based Model for Soft Clays. *Master's thesis*, Norwegian University of Science and Technology, Trondheim, Norway

Bjerrum, L. (1967). Engineering geology of Norwegian normally-consolidated marine clays as related to settlements of buildings. *Géotechnique*, **17**(2): 83-118.

Conn, A.R., Scheinberg, K., and Vicente, L.N. (2009). *Introduction to derivative-free optimization*. SIAM Publications (Philadelphia).

Desai, C., and Zhang, D. (1987). Viscoplastic model for geologic materials with generalized flow rule. *International Journal for Numerical and Analytical Methods in Geomechanics*, **11**(6): 603-620.

di Prisco, C., and Imposimato, S. (1996). Time dependent mechanical behaviour of loose sands. Mechanics of Cohesive-frictional Materials: *An International Journal on Experiments, Modelling and Computation of Materials and Structures*, **1**(1): 45-73.

Fang, H.-Y. (2013). *Foundation engineering handbook*. Springer Science & Business Media, New York. Doi:10.1007/978-1-4757-5271-7.

Fodil, A., Aloulou, W., and Hicher, P. (1998). Viscoplastic behaviour of soft clay. *Pre-failure deformation behaviour of geomaterials*: 195.

Fredlund, D.G. (1967). *Comparison of soil suction and one-dimensional consolidation characteristics of a highly plastic clay.* National Research Council Canada, Division of Building Research. (pp. 193-201).

Goodman, R. (1974). The mechanical properties of joints. In Proceedings of the third international congress international society of rock mechanics Denver, Colorado. *National Academy of Sciences*, Washington, DC. (pp. 127-140).

Helwany, S. (2007). *Applied soil mechanics with ABAQUS applications*. John Wiley & Sons, Inc, the United States.

Hewage, R.E. (2018). An experimental study on time-dependent behaviour of reconstituted clayey soils in 1D and triaxial compression. *PhD thesis*, The University of Calgary, Alberta, Canada.

Hicher, P. (2016). Experimental study of viscoplastic mechanisms in clay under complex loading. *Géotechnique*, **66**(8): 661-669.

Kabbaj, M., Tavenas, F., and Leroueil, S. (1988). In situ and laboratory stress–strain relationships. *Géotechnique*, **38**(1): 83-100.

Karim, M.R., and Gnanendran, C. (2008). Review of visco-plastic soil models for predicting the performance of embankments on soft soils. *In Proceedings of the 12th International Conference of International Association for Computer Methods and Advances in Geomechanics*, Goa, India. (pp. 1-6).

Katona, M.G., and Mulert, M.A. (1984). *A viscoplastic cap model for soils and rock*. C.S. Desai and R.H. Gallagher (Editors), *Mechanics of Engineering Materials*, Wiley, New York.

Kurz, D. (2014). Understanding the effects of temperature on the behaviour of clay. *PHD thesis,* The University of Manitoba, Manitoba*,*Canada

Lacerda, W. (1973). Stress relaxation in soils. Proc. *8th ICSMFE*, Moscow: 221-227.

Leroueil, S., Kabbaj, M., Tavenas, F., and Bouchard, R. (1985). Stress–strain–strain rate relation for the compressibility of sensitive natural clays. *Géotechnique*, **35**(2): 159-180.

Liingaard, M., Augustesen, A., and Lade, P.V. (2004). Characterization of models for time-dependent behavior of soils. *International Journal of Geomechanics*, **4**(3): 157-177.

Marques, M.E.S., Leroueil, S., and Soares de Almeida, M.d.S. (2004). Viscous behaviour of St-Roch-de-l'Achigan clay, Quebec. *Canadian Geotechnical Journal*, **41**(1): 25-38.

Mesri, G., Kelly, W., Vallee, R., and Andersland, O. (1973). Ceofficient of secondary compression (discussion). *Journal of Soil Mechanics & Foundations Div*, **99**(Proc Paper).

Oka, F. (1988). Elasto-viscoplastic constitutive models for clays. *In* Proc. Int. *Conf. Rheology and Soil Mech.* (pp. 12-28).

Perzyna, P. (1963). The constitutive equation for work-hardening and rate sensitive plastic materials. *In Proc. Vibrational Problems*. (pp. 281-290).

Picornell, M., and Nazarian, S. (1992). Behavior of unsaturated clayey soils at high strain rates. *Final report for contract NO. F49620-89-C-0077*, Center for geotechnical & highway materials research, The University of Texas at El Paso.

Picornell, M., and Nazarian, S. (1996). Undrained Creep Behavior of Clayey Soils. *Final report for contract NO. F49620-92-J-0294*, Center for geotechnical & highway materials research, The University of Texas at El Paso.

Resende, L., and Martin, J.B. (1985). Formulation of Drucker-Prager cap model. *Journal of Engineering Mechanics*, **111**(7): 855-881.

Roscoe, K.H., and Burland, J. (1968). On the generalized stress-strain behaviour of wet clay. Engineering plasticity, J. Heyman and F. A. Lekie, eds., Cambridge University Press, London, England. (pp. 535-609).

Shin, H., Kim, J.-B., Kim, S.-J., and Rhee, K.Y. (2015). A simulation-based determination of cap parameters of the modified Drucker–Prager cap model by considering specimen barreling during conventional triaxial testing. *Computational Materials Science*, **100**: 31-38.

Sing, A., and Mitchell, J. (1968). General stress–strain-time functions for soils. *Soil Mechanics and Foundation Division*, **94**: 21-46.

Suhonen, K. (2018). Creep of soft clay. *Master's thesis*, Aalto University, Greater Helsinki, Finland.

Suklje, L. (1957). The analysis of the consolidation process by the isotaches method. *In Proceedings of the 4th International Conference on Soil Mechanics and Foundation Engineering*, London. (pp. 200-206).

Taiebat, H., and Carter, J. (2000). Numerical studies of the bearing capacity of shallow foundations on cohesive soil subjected to combined loading. *Géotechnique*, **50**(4): 409-418.

Tavenas, F. (1977). Effects of stresses and time on the yielding of clay. *In Proceedings of the 9th ICSMFE.* (pp. 319-326).

Tavenas, F., Leroueil, S., Rochelle, P.L., and Roy, M. (1978). Creep behaviour of an undisturbed lightly overconsolidated clay. *Canadian Geotechnical Journal,* **15**(3): 402-423.

Terzaghi, K. (1951). *Theoretical soil mechanics*. John Wiley & Sons, Inc, the United States.

Vu, H.Q., Hu, Y., and Fredlund, D.G. (2007). Analysis of soil suction changes in expansive Regina clay. *Proceedings of GeoOttawa2007*, Ottawa, Ont.

Wong, C.K., Wan, R.G., and Wong, R.C. (2018). Methodology for Estimating Creep Deformation from Consolidation Deformation in 1D Compression. *International Journal of Geomechanics*, **18**(6): 04018042.

Yin, J.-H., and Graham, J. (1989). Viscous–elastic–plastic modelling of one-dimensional time-dependent behaviour of clays. *Canadian Geotechnical Journal*, **26**(2): 199-209.

Yin, J.-H. (1990). Constitutive modelling of time-dependent stress-strain behaviour of soils. *PHD thesis*, The University of Manitoba, Manitoba, Canada.

Yin, J.-H., and Graham, J. (1994). Equivalent times and one-dimensional elastic viscoplastic modelling of time-dependent stress–strain behaviour of clays. *Canadian Geotechnical Journal*, **31**(1): 42-52.

Yin, J.-H., and Graham, J. (1999). Elastic viscoplastic modelling of the time-dependent stress-strain behaviour of soils. *Canadian Geotechnical Journal*, **36**(4): 736-745.

Yin, Z.-Y., Chang, C.S., Karstunen, M., and Hicher, P.-Y. (2010). An anisotropic elastic–viscoplastic model for soft clays. *International Journal of Solids and Structures*, **47**(5): 665-677.

Yin, Z.-Y., Karstunen, M., Chang, C.S., Koskinen, M., and Lojander, M. (2011). Modeling time-dependent behavior of soft sensitive clay. *Journal of geotechnical and geoenvironmental engineering*, **137**(11): 1103-1113.

Yin, Z., Hicher, P.Y., Riou, Y., and Huang, H.-W. (2006). An elasto-viscoplastic model for soft clay. *In Soil and Rock Behavior and Modeling-Proceeding of the Geoshanghai Conference, vol*. 150, Shanghai, Geotechnical Special Publication. (pp. 312-319).